(Molecular Devices, Tokyo, Japan) with excitation at 480 nm and emission at 530 nm.

Mouse model of acute lung injury

Paraquat treatment. Wild-type (WT) mice (Charles River Japan, Yokohama) and C57 BJ/6 background *VASH1* (+/−) KO mice [3,10] of C57 BJ/6 background (9 to 10 weeks of age) were used in this study. Paraquat was dissolved in phosphate-buffered saline (5 mg/mL) and injected intraperitoneally at the dosage of 50 mg/kg body weight [11]. To evaluate the protective effect of VASH1, we used purified AdVASH1. Purified AdLacZ was used for the control [2,12]. Mice were anesthetized with ketamine (0.1 mg/g) and xylazine (0.01 mg/g) administered by intraperitoneal injection and then intubated orotracheally with a 22-G angiocatheter. A total of 75 microl of AdVASH1 or AdLacZ, containing 1×10^9 plaque-forming units, was injected into each mouse ototracheally [13]. Paraquat was injected intraperitoneally at the dosage of 50 mg/kg body weight 72 hours after administration of the adenovirus. The mice were followed periodically over 10 days, and the number of deaths was recorded. At the end of 10 days, all remaining mice were terminated.

β-gal staining. Mice were sacrificed 2 days after the intratracheal administration of PBS or AdLacZ. The pulmonary circulation was flushed with ice-cold 2% buffered paraformaldehyde, 0.2% glutaraldehyde, and 0.02% NP40 via the right ventricle. The lung blocks were inflation-fixed through the trachea with 2% buffered paraformaldehyde/PBS for 2 hours at room temperature. Thereafter, the lungs were incubated at room temperature in 1 mg/mL X-gal, 5 mmol/L potassium ferricyanide crystalline, 5 mmol/L potassium ferricyanide trihydrate, 2 mmol/L magnesium chloride, and 0.1% NP40 and then embedded in paraffin. Four-micrometer sections were prepared and then counterstained with nuclear fast red.

Histological analysis of the lungs. Mice were sacrificed 2 days after paraquat administration. The lungs were inflation-fixed through the trachea with 4% buffered paraformaldehyde/PBS overnight at 4°C, and then embedded in paraffin. Four-micrometer sections were prepared and then stained with hematoxylin and eosin (H&E).

For the staining of 8-OHdG, sections were incubated with the anti-8-OHdG antibody overnight at 4°C at a 1:20 dilution. They were then incubated in 10% H_2O_2/methanol to block endogenous peroxidase activity. The secondary antibody reaction was performed with biotin-conjugated anti-mouse IgG for 40 min at room temperature. Streptavidin-biotin peroxidase complex formation was performed for 30 min at room temperature. The peroxidase products were visualized by using diaminobenzidine.

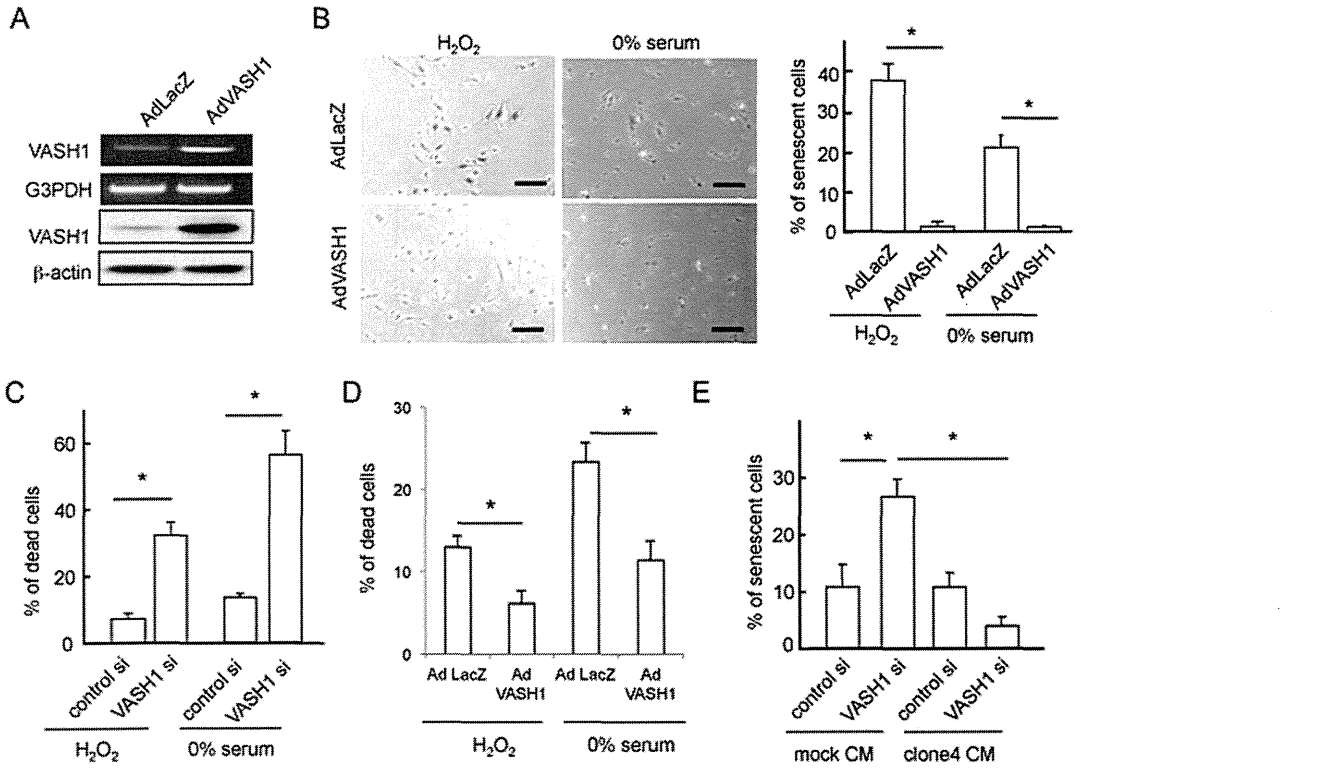

Figure 2. Overexpression of VASH1 inhibits premature senescence and cell death of HUVECs induced by cellular stresses. (A) HUVECs were infected with AdVASH1 or AdLacZ. After a 24-hour incubation, RT-PCR and Western blotting for VASH1 were performed. (B) HUVECs infected with AdVASH1 or AdLacZ were exposed to 100 μmol/L H_2O_2 for 1 hour, followed culture for 24 hours (on the left) or to 0% FCS/αMEM 24 hours (on the right). After a 6-day culture, SA β-gal staining was performed. Scale bars are 250 microm. SA β-gal-positive HUVECs were quantified, and the % of senescent cells was calculated (*P<0.01, N=3). (C) HUVECs were transfected with VASH1 siRNA or control siRNA. After a 24-hour incubation, HUVECs were exposed to 100 μmol/L H_2O_2 or to 0% FCS/αMEM for 24 hours, and then the trypan blue exclusion assay was performed. Blue-stained cells were quantified, and the % of dead cells was calculated (*P<0.01, N=3). (D) HUVECs infected with AdVASH1 or AdLacZ were exposed to 100 μmol/L H_2O_2 for 48 hours or to 0% FCS/αMEM for 24 hours for 24 hours; and then the trypan blue exclusion assay was performed (*P<0.01, N=3). (E) HUVECs were transfected with VASH1 siRNA or control siRNA. After a 24-hour incubation, the growth medium was replaced with 50% conditioned medium derived from mock or VASH1 over-expressing MS1 clone 4. After a 24-hour incubation, the trypan blue exclusion assay was performed (*P<0.01, N=3). All the studies were repeated at least 3 times to confirm the reproducibility.
doi:10.1371/journal.pone.0046459.g002

Determination of protein and cell counts in the broncheoalveolar lavage fluid (BALF). Broncheoalveolar lavage was performed by intratracheal injection of PBS (0.7 ml) for 2 times. BALF was collected and centrifuged at 400 g for 5 min at 4°C. The recovered fluid was processed for determination of protein concentration (DC Protein Assay; Bio-Rad Laboratories, Inc, CA). The pelleted cells were resuspended in 1 ml PBS and counted.

Calculations and statistical analysis

Data were expressed as means ± SDs. The statistical significance of differences between groups was evaluated by use of the unpaired ANOVA, and P values were calculated by performing the unpaired Student's t test. The significance between survival curves was analyzed by Kaplan-Meier survival analysis with log-rank testing. A value of $P<0.05$ was the criterion for significance.

Results

VASH1 protects ECs from premature senescence and stress-induced cell death

To understand the function of VASH1, we applied siRNA-mediated knock-down of VASH1 expression in HUVECs (Fig. 1A). We noticed that HUVECs lacking VASH1 became flatter under the basal condition (Fig. 1B). As this phenotype resembles that of senescent cells, we assessed the cellular senescence. There was a significant increase in SA β-gal reactivity in HUVECs lacking VASH1 (Fig. 1B). As ATM is known to be phosphorylated during premature senescence of ECs [14], we examined the level of phosphorylated ATM (p-ATM) in HUVECs lacking VASH1 and found an increase in it (Fig. 1C). It was described that autophagy is associated with premature senescence [15]. Immunostaining for LC3, a marker of autophagy, revealed autophagy in HUVECs lacking VASH1 (Fig. 1D). These results indicate that the knock-down of VASH1 caused the premature senescence of ECs. Although VASH1 lacks a classical signal sequence, it is secreted by binding to the small vasohibin-binding protein [16]. Accordingly, treatment of HUVECs with blocking monoclonal anti-VASH antibody induced a similar senescence phenotype (Fig. 1E), suggesting the importance of secreted VASH1 in protecting against cellular senescence.

We next overexpressed the human *VASH1* gene in HUVECs (Fig. 2A). Basal expression of VASH1 in ECs varies depending on the culture condition, as sparse HUVECs express less whereas subconfluent to confluent HUVECs express more VASH1 [3]. We therefore used sparse HUVECs for the overexpression. When those HUVECs were exposed to H_2O_2 or serum starvation, the AdVASH1-infected HUVECs exhibited resistance to premature senescence (Fig. 2B). We examined cell death after the exposure to cellular stresses. When HUVECs lacking VASH1 were exposed to H_2O_2 or serum starvation, they were vulnerable and easier to be

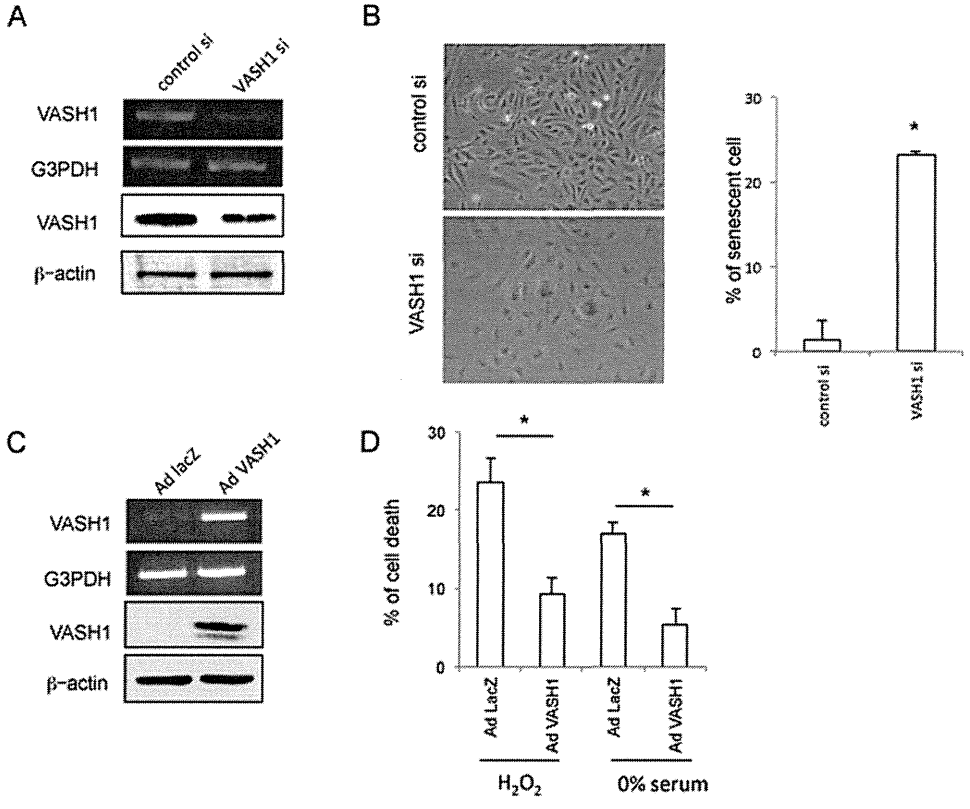

Figure 3. VASH1 inhibits premature senescence and cell death of HAECs. (A) HAECs were transfected with VASH1 siRNA or control siRNA. After a 24-hour incubation, RT-PCR and Western blotting for VASH1 were performed. (B) After a 6-day incubation, SA beta-gal staining was performed on HAECs that had been transfected with VASH1 siRNA or control siRNA. SA beta-gal-positive HAECs were quantified, and the % of senescent cells was calculated (*$P<0.01$, $N=3$). (C) HAECs were infected with AdVASH1 or control AdLacZ. After a 24-hour incubation, RT-PCR and Western blotting for VASH1 were then performed. (D) HAECs infected with AdVASH1 or control AdLacZ were exposed to 100 μmol/L H_2O_2 or to 0% FCS/DMEM for 24 hours. The trypan blue exclusion assay was performed to judge cell death (*$P<0.01$, $N=3$). All the studies were repeated at least 3 times to confirm the reproducibility.
doi:10.1371/journal.pone.0046459.g003

killed by those stresses (Fig. 2C). In contrast, HUVECs overexpressing VASH1 were resistant to those cellular stresses (Fig. 2D). Importantly, stress-induced HUVEC premature senescence could be prevented by medium conditioned by stable VASH1 transfectant (Fig. 2E).

We applied HAECs as another primary ECs. Identical to HUVECs, HAECs became senescent when VASH1 was knocked-down (Fig. 3A and B). Alternatively, HAECs became resistant to cellular stresses when VASH1 was overexpressed (Fig. 3C and D). We previously established stable human VASH1 transfectants of MS1 [8]. Those stable transfectants were also resistant to cellular stresses (Figure S1 A and B).

Collectively, the above data showed VASH1 to protect ECs from premature senescence and to make them resistant to stress-induced cell death.

VASH1 protein level is determined via HuR-mediated posttranscriptional regulation

We examined whether cellular stress modulated the expression of VASH1 in ECs. We observed that cellular stress increased VASH1 protein level at 1–6 hour time points without the increase of VASH1 mRNA (Fig. 4A), indicating that post-transcriptional regulation might operate to increase the level of VASH1 protein when ECs were exposed to stress. Hu proteins are RNA-binding proteins that bind to AU-rich elements (AREs) in the 3′ untranslated region (UTR) of mRNAs [17]. We could show such elements in the 3′ UTR of VASH1 (Fig. 4B). Among Hu proteins, HuR is mostly related to cellular stress responses [18]. ChIP assay proved that HuR protein bound to this region in HUVECs (Fig. 4C). Furthermore, the knock-down of HuR abrogated the increase in VASH1 protein upon cellular stress in HUVECs (Fig. 4D). These results suggest that VASH1 in the ECs was targeted by HuR.

VASH1 protects ECs via the induction of SOD2 and SIRT1

VEGF produced by ECs is reported to be a survival factor for ECs themselves [19]. SU5416, a VEGF receptor kinase inhibitor, did not affect the basal expression of VASH1 in HUVECs, but induced EC death (Figure S2 A and B). This EC death could be diminished by AdVASH1, but the senescence phenotype induced by VASH1 siRNA could not be reversed by exogenous VEGF (Figure S2B and C). These results suggest that the effect of VASH1 may not have involved the VEGF signaling.

One of the major causes of stress-induced premature senescence is ROS [20]. We could show that cellular ROS was significantly higher in HUVECs lacking VASH1 (Fig. 5A). We sought the reason for this increase in the ROS level in HUVECs lacking VASH1. Among various antioxidants tested, SOD2 was found to be down-regulated in HUVECs lacking VASH1 (Fig. 5B).

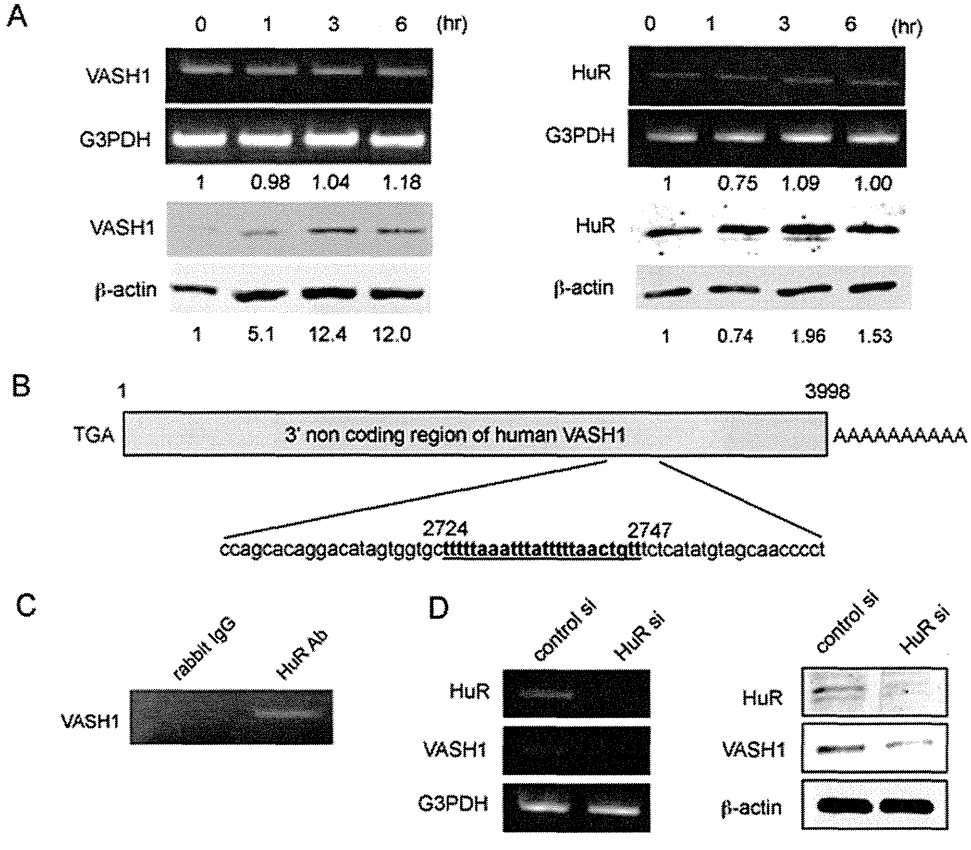

Figure 4. HuR increases VASH1 protein level in HUVECs. (A) HUVECs were incubated in 0% FCS/αMEM, and total RNA and protein were extracted at the indicated time points. Thereafter, RT-PCR and Western blotting for VASH1 were performed. Values below each band represent the mean fold change in RNA or protein expression level compared with the cognate zero time. (B) The AU-rich element (ARE) in the 3′ non coding region of the VASH1 gene is shown. (C) Immunoprecipitation and reverse transcription-polymerase chain reaction were performed as described in Materials and Methods. (D) HUVECs were transfected with HuR siRNA or control siRNA. After a 24- hour incubation, total RNA and protein were extracted; and then RT-PCR for HuR and Western blotting for VASH1 were performed. All the studies were repeated at least 3 times to confirm the reproducibility.
doi:10.1371/journal.pone.0046459.g004

Moreover, when ROS were quenched by NAC, premature senescence was partly but significantly inhibited in HUVECs lacking VASH1 (Fig. 5C). Alternatively, overexpression of VASH1 decreased the ROS level when exposed to cellular stresses, and up-regulated SOD2 in HUVECs (Fig. 5D and E). However, when this increase of SOD2 was knocked-down by siRNA, the protective effect of VASH1 on premature senescence was significantly abrogated (Fig. 5F).

NAC partly inhibited premature senescence (Fig. 5B). Thus we reasoned that some additional mechanism might be involved. In addition to antioxidants, attention has been recently paid to the protective protein named SIRT1 [21]. Moreover, the synthesis and function of SIRT1 are related to HuR and ATM [22]. Therefore we tested the SIRT1 protein level. The knockdown of VASH1 significantly decreased the level of SIRT1 protein and its activity as well (Fig. 6A and B). However, if this reduced SIRT1 activity was enhanced by SIRT1 activator 3, the premature senescence of HUVECs lacking VASH1 was notably suppressed (Fig. 6C). Interestingly, the knock-down of SIRT1 increased the VASH1 protein level (Fig. 6D). Alternatively, when VASH1 was overexpressed in HUVECs by AdVASH1, SIRT1 protein significantly increased (Fig. 6E). Moreover, when SIRT1 was knocked-down, the VASH1-mediated protection against stress-induced premature senescence and cell death vanished (Fig. 6E and F).

Collectively, the above data showed VASH1 to protect ECs via the induction of SOD2 and SIRT1.

VASH1 protects mice from death with acute lung injury induced by paraquat treatment

To prove the protective role of VASH1 *in vivo*, we applied paraquat intoxication to mice. Paraquat is used as a redox cycler

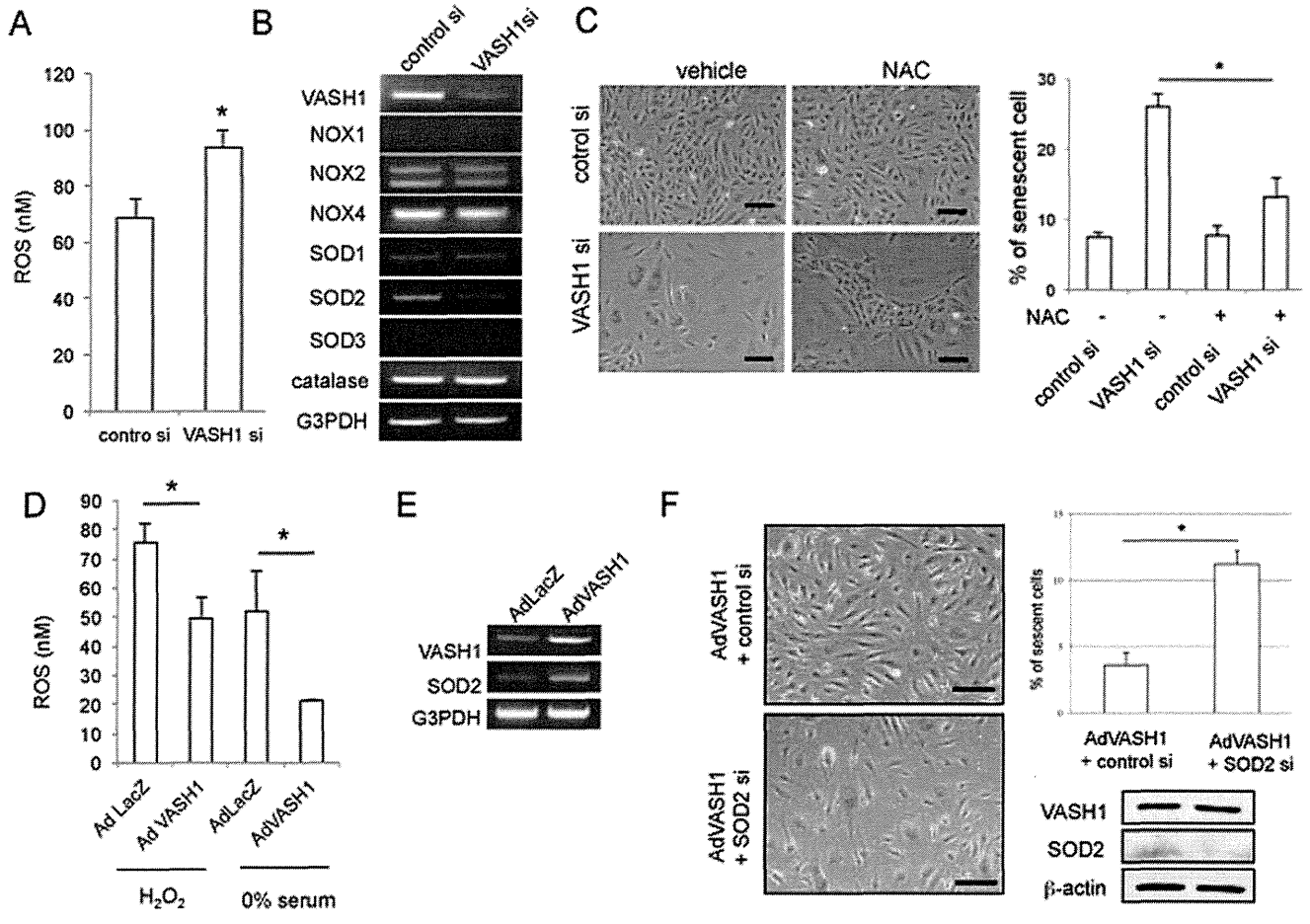

Figure 5. VASH1 controls SOD2 level and decreases ROS level in HUVECs. (A) HUVECs were transfected with VASH1 siRNA or control siRNA. After a 24-hour incubation, cellular ROS was determined as described in Materials and Methods (*$P<0.01$, $N=3$). (B) HUVECs were transfected with VASH1 siRNA or control siRNA. Twenty-four hours later, RT-PCR for the indicated genes was performed. (C) HUVECs were transfected with VASH1 siRNA or control siRNA in the presence or absence of 50 μmol/L NAC. After a 12-hour incubation, the culture medium was replaced with growth medium containing vehicle or 50 μmol/L NAC. After a 6-day culture, SA β-gal staining was performed. Scale bars are 250 μm. SA β-gal-positive HUVECs were quantified, and the % of senescent cells was calculated (*$P<0.01$, $N=3$). (D) HUVECs were infected with AdVASH1 or AdLacZ. After a 24-hour incubation, the cells were exposed to 100 μmol/L H_2O_2 for 1 hour or to 0% FCS/αMEM for 6 hours. Thereafter, the cellular ROS level was determined (*$P<0.01$, $N=3$). (E) HUVECs were infected with AdVASH1 or AdLacZ. After a 24-hour incubation, RT-PCR for VASH1 and SOD2 was performed. (F) HUVECs were infected with AdVASH1 or AdLacZ. After a 24-hour incubation, HUVECs were then transfected with SOD2 siRNA or control siRNA. After a subsequent 24-hour incubation, the cells were exposed to 100 μ mol/L H_2O_2 for 1 hour followed by a 48-hour incubation in growth medium. Scale bars are 250 μm. SA β-gal staining and Western blotting for VASH1 and SOD2 were then performed. SA β-gal-positive HUVECs were quantified, and the % of senescent cells was calculated (*$P<0.01$, $N=3$). All the studies were repeated at least 3 times to confirm the reproducibility.

doi:10.1371/journal.pone.0046459.g005

to stimulate superoxide production; and it causes acute organ injury mainly in the lungs [23]. Over a 10-day period following the administration of paraquat, the death rate even in the *VASH1* (+/−) KO mice was higher than that in the WT mice; and the survival curves for the WT and *VASH1* (+/−) KO mice were thus significantly different (Fig. 7A). Lungs were obtained 48 hours after the paraquat administration and histological analysis was performed. Cellular infiltration, and interstitial edema were evident in *VASH1* (+/−) KO mice (Fig. 7B, on the left). Immunohistochemistry for 8-OHdG revealed that DNA damage in *VASH1* (+/−) KO (Fig. 7B, on the right). Moreover, protein levels and cell counts in the bronchoalveolar lavage fluid (BALF) were significantly increased in *VASH1* (+/−) KO mice (Fig. 7C).

Staining for β-gal activity indicated that the intratracheally administered AdLacZ had been delivered to entire bronchial epithelium and some vessels (Figure S3 A and B). When AdVASH1 was intratracheally administered, VASH1 protein synthesis was detected in the lungs for at least 10 days (Figure S3C). We then tested whether the intratracheal administration of AdVASH1 could protect mice from the paraquat-induced lung injury. Over the same 10-day period, the deaths in the group of *VASH1* (+/−) KO mice administered AdVASH1 were significantly fewer than in the group administered AdLacZ (Fig. 7D). Histological analysis of the lungs revealed that the AdVASH1 treatment attenuated the acute lung injury and DNA damage in *VASH1* (+/−) KO mice given AdVASH1 compared with that in those administered AdLacZ (Fig. 7E). Protein levels and cell counts in the BALF were significantly less in the former than in the latter (Fig. 7F). To verify the involvement of SOD2 and SIRT1 in the effect of VASH1 *in vivo*, we investigated those proteins in the lung tissue, and found that AdVASH1 increased SOD2 and SIRT1 contents in the lungs (Fig. 7G). Since the intratracheal administration of adenovirus vector tranfered gene mainly in bronchial epithelium, we assumed that VASH1 synthesized by bronchial epithelium affect on neighboring ECs. However, VASH1 might affect the bronchial epithelium as well. NHBECs did not express

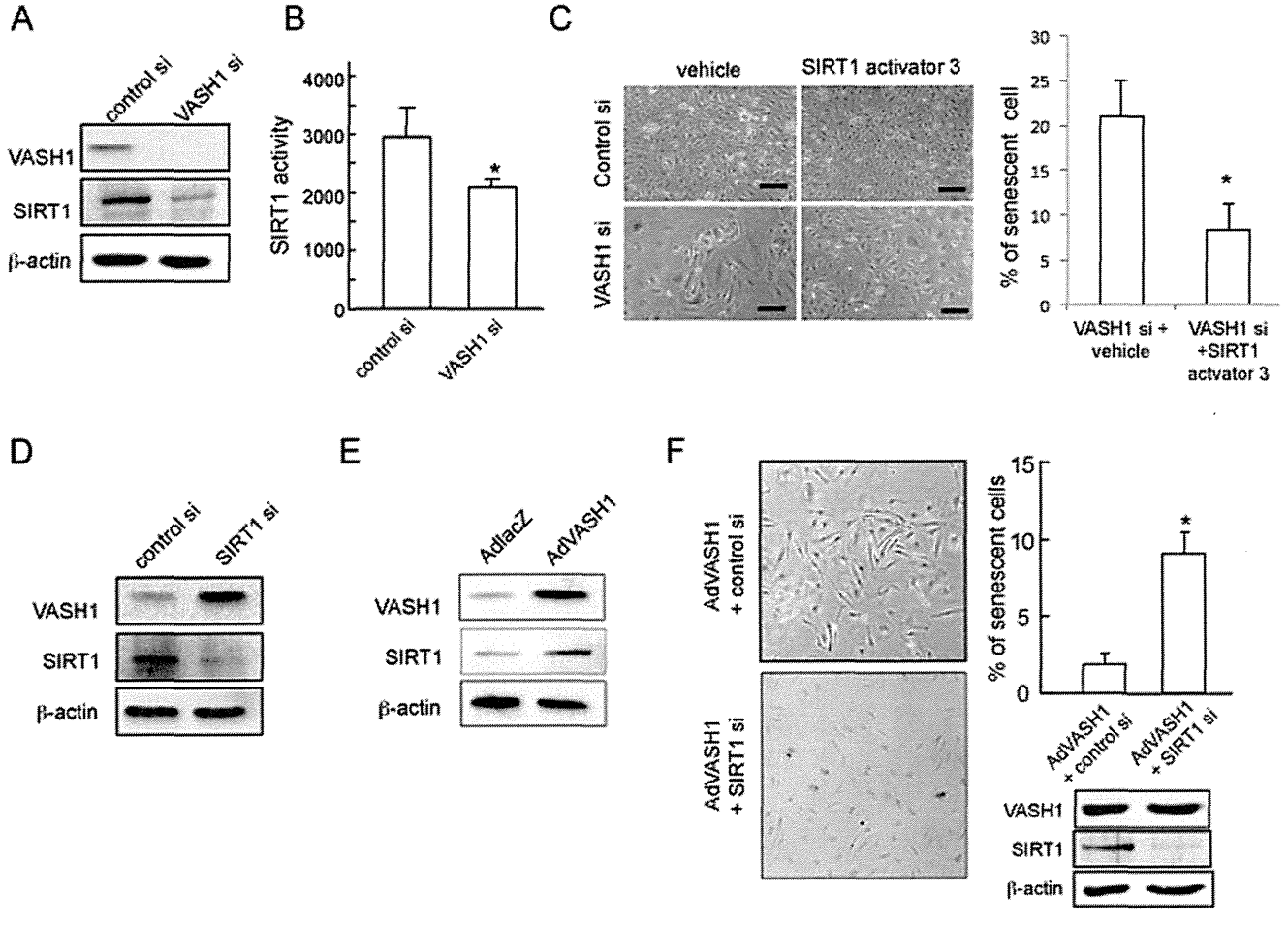

Figure 6. VASH1 controls SIRT1 level and increases stress resistance of HUVECs. (A) HUVECs were transfected with VASH1 siRNA or control siRNA. After a 72-hour incubation, Western blotting for VASH1 and SIRT1 was performed. (B) HUVECs were transfected with VASH1 siRNA or control siRNA. After a 24-hour incubation, SIRT1 activity was determined (*P<0.01, N = 3) (C) HUVECs were preteated with vehicle or 5 μmol/L SIRT1 activator 3 for 12 hours, and then transfected with VASH1 siRNA or control siRNA. After a 6-day incubation, SA β-gal staining was performed. Scale bars are 100 μm. SA β-gal-positive HUVECs were quantified, and the % of senescent cells was calculated (*P<0.01, N = 4). (D) HUVECs were transfected with SIRT1 siRNA or control siRNA. After a 72-hour incubation, Western blotting for VASH1 and SIRT1 was performed. (E) HUVECs were infected with AdVASH1 or AdLacZ. After a 72-hour incubation, Western blotting for VASH1 and SIRT1. (F) HUVECs were infected with AdVASH1. After a 24-hour incubation, HUVECs were then transfected with SIRT1 siRNA or control siRNA. After a subsequent 24-hour incubation, the cells were exposed to 100 μmol/L H_2O_2 for 1 hour followed by a 48-hour incubation in growth medium. Scale bars are 250 μm. SA β-gal staining and Western blotting for VASH1 and SIRT1 were then performed. β-gal-positive HUVECs were quantified, and the % of senescent cells was calculated (*P<0.01, N = 3). All the studies were repeated at least 3 times to confirm the reproducibility.
doi:10.1371/journal.pone.0046459.g006

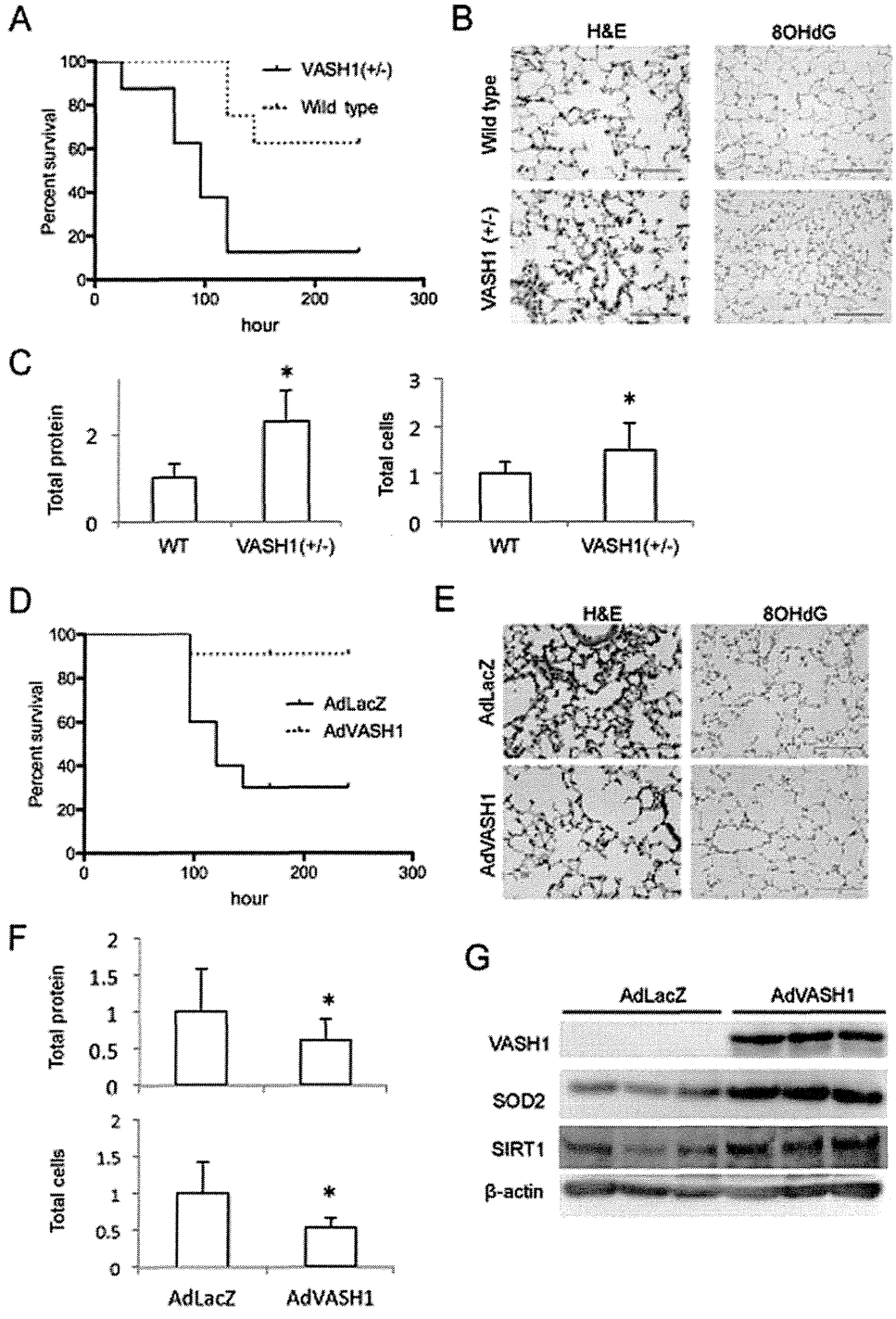

Figure 7. VASH1 protects mice from death with acute lung injury induced by paraquat treatment. (A) Paraquat was administered to WT (N = 8, dotted line) or *VASH1* (+/−) mice (N = 8, solid line), and the survival was observed over 10 days. Kaplan-Meier survival analysis showed significant difference. (B) Two days after paraquat administion, histological analyses of the lungs were performed. H&E staining is shown on the left, and immunostaining for 8-OHdG on the right. (C) Two days after paraquat administration, total protein and number of cells in the BALF were determined. *Significant difference (N = 7). (D) Paraquat was administered to *VASH1* (+/−) mice intratracheally infected with AdVASH1 (N = 10, dotted line) or AdLacZ (N = 11, solid line), and the survival was observed over 10 days. Kaplan-Meier survival analysis showed significant difference. (E) Two days after paraquat administion to AdLacZ or AdVASH1 mice, histological analyses of lungs were performed. H&E staining is shown on the left; and immunostaining fo 8-OHdG, on the right. (F) Two days after paraquat administration, BALF was collected; and total protein and number of cells in the BALF were determined. *Significant difference (N = 10). (G) Three days after the intratracheal infection of mice with AdVASH1 or AdLacZ, their lungs were removed and tissue extracts prepared. Western blotting for VASH1, SOD2, and SIRT1 in the extracts was performed.
doi:10.1371/journal.pone.0046459.g007

endogenous VASH1 (Figure S4A). In addition, the overexpression of VASH1 in NHBECs did not alter the level of SOD2 and SIRT1 (Figure S4B) nor the cell death after the treatment with H_2O_2 (Figure S4C). We therefore judge that the protective action of VASH1 in the paraquat-induced acute lung injury occurred mainly through ECs.

Discussion

Our previous studies on VASH1 were focused on the inhibition of angiogenesis. Here we noticed, to our surprise, that the knock-down of basal VASH1 expression resulted in the premature senescence of ECs. We extended our study and revealed for the first time that VASH1 protected ECs from premature senescence and cell death when the cells were exposed to oxidative or serum-starvation stress. Angiogenesis inhibition generally causes vascular regression by inducing EC death, which regression may also result in proteinuria and hypertension *in vivo* [24]. We noted earlier that VASH1 neither instigates such vascular regression nor causes proteinuria and hypertension [25,26]. Our present results further highlight the uniqueness of VASH1 in that it not only inhibited angiogenesis but also enhanced the maintenance of ECs by strengthening resistance against stress. The presice mechanism of the action of VASH1 remains to be elucidated.

VASH1 mRNA is induced by stimulation with angiogenic factors such as VEGF and FGF-2 via the activation of PKC-δ [27]. Here we observed that the VASH1 protein level increased without the increase in VASH1 mRNA when ECs were exposed to cellular stress, suggesting the posttranscriptional gene regulation. One of the important mechanisms of posttranscriptional regulation is the rapid degradation of mRNAs signaled by AREs in their 3′ UTR. The Hu family of RNA-binding proteins binds to AREs in the 3′UTRs of the target mRNAs, prevents their degradation, and enhances their translation [18]. There are 4 members of Hu proteins; HuB, HuC, HuD and HuR. Whereas HuB, HuC, and HuD are selectively expressed in the nervous system and play roles in neuronal differentiation and plasticity, HuR is ubiquitously expressed and exhibits numerous functions mostly related to cellular stress responses [18]. Thus, we consider the stress-induced VASH1 protein synthesis to have been regulated by HurR.

Here we gave evidence for 2 proteins as targets of VASH1 for the maintenance of ECs, the first being SOD2. The SOD family forms the major antioxidant defense system, which consists of 3 members: SOD1 as the cytoplasmic Cu/Zn-SOD, SOD2 as the mitochondrial Mn-SOD, and SOD3 as the extracellular Cu/Zn-SOD [28]. Because of its localization in mitochondria, SOD2 is the first line of defense against oxidative stress [29]. ECs are known to express a high level of SOD2 [30], and SOD2 is thought to play a principal role in protecting the vascular system from oxidative stress generated by various pathophysiological processes [31]. The second target of VASH1 we discovered was SIRT1. SIRT1 is a member of mammalian NAD^+-dependent deacetylase family. Among them, SIRT1 is widely expressed, and is now considered to be responsible for the protection of cells from various types of stress [32]. Particularly, a number of reports indicate that vascular SIRT1 protects vessels from various vascular diseases including atherosclerosis and diabetic vascular complications [33–36]. The knock-down of VASH1 decreased the expression of SIRT1, whereas the knock-down of SIRT1 increased the expression of VASH1 in ECs. This may suggest that VASH1 lays upstream of SIRT1 in the axis of VASH1-SIRT1 in ECs. SIRT1 is expressed in ECs during angiogenesis [37]. The correlation of VASH1 and SIRT1 in the regulation of angiogenesis needs to be determined in future.

As mentioned earlier, angiogenesis inhibitors induce EC death and vascular regression [24]. Hence, the most intriguing aspect of VASH1 is simultaneous angiogenesis inhibition and EC protection. It is well documented that inflammatory cells form dense infiltrates at the site of angiogenesis and that oxidative stress is the major characteristic of such inflammatory conditions [38,39]. Moreover, ROS can be one of the mediators of angiogenesis as well [27]. For that reason, we propose that the function of VASH1 is to halt angiogenesis and stabilize neo-vessels.

VASH1 is highly expressed in ECs at sites of angiogenesis. However, besides its presence there, we noticed previously that VASH1 protein is detectable in arterial ECs under the basal condition [40]. Arterial ECs are exposed to various physical forces. Moreover, oxidative stress-induced DNA damage is thought to play an important role in vascular senescence and senescence-related vascular diseases [41]. We therefore suggest that such VASH1 in the arterial wall is available there for the protection of vessels. Indeed we noted in earlier studies that VASH1 can prevent intimal thickening of arteries as well as diabetic renal injury [12,42].

The lungs are the organ with the highest exposure to ambient air among all of the organs in the body. Because of its large alveolus surface and affluent blood perfusion, the lung tissue is most susceptible to oxidative injury. Here we used Paraquat to induce acute lung injury and showed that the intrabronchial sdministration of AdVASH1 protected lungs from acute lung injury. Since the intratracheal administration of adenovirus vector tranfered gene mainly in bronchial epithelium, we assumed that VASH1 synthesized by bronchial epithelium should affect on neighboring ECs in a paracrine manner. The excessive oxidative stress is thought to be one of the major causes of various lung diseases including chronic obstructive pulmonary diseases (COPD), pulmonary hypertension, and the post-reperfusion injury of transplanted lungs [43–45]. Moreover, there are several reports describing the relationship among SOD2, SIRT1, and COPD [46–48]. It would be therefore interesting to see if there is any relationship between those pulmonary diseases and VASH1.

In summary, our present study revealed that VASH1 not only inhibited angiogenesis but also enhanced the maintenance of ECs by strengthening their resistance against stress. We showed SOD2 and SIRT1 to be targets of VASH1 in ECs for strengthening this resistance. The close relationship among VASH1, SOD2 and SIRT1 may indicate the protective value of VASH1 in the vascular system.

Supporting Information

Figure S1 VASH1 over-expression inhibits the cell death of MS1 cells induced by cellular stresses. Stable VASH1-expressing MS1 clones and mock MS1 transfectants were exposed to 200 μmol/L H_2O_2 (A) or serum starved (0% FCS/DMEM, B) for 24 hours. The trypan blue exclusion assay was then performed to judge cell death. Blue-stained cells were quantified, after which the % of dead cells was calculated. Values are the ratio of blue-stained cells to total cells, and are the means and SDs of 3 wells. *Significant difference compared with the value for the corresponding mock. (TIFF)

Figure S2 VASH1 protects HUVEC death by the treatment with a VEGF receptor inhibitor. (A) HUVECs were incubated in growth medium containing SU5416. Total RNA and protein were extracted from the cells at the indicated times, and then RT-PCR and Western blotting for VASH1 were performed.

(B) HUVECs were infected with AdVASH1 or AdLacZ. After a 24-hour incubation, SU5416 was added. After an additional 3 days' incubation, the trypan blue exclusion assay was performed. Blue-stained cells were quantified, and the % of dead cells was calculated. *Significant difference compared with the value for the corresponding AdLacZ. (C) HUVECs were transfected with VASH1 siRNA or control siRNA. In some case, VEGF (1 nmol/L) was added to HUVECs that had been transfected with VASH1 siRNA. The cells were cultured for 3 days, and observed by phase-contrast microscopy.
(TIFF)

Figure S3 Intratracheal administration of adenovirus vector. (A) PBS (left photo) or AdVASH1 (right photo) was intratracheally administered to WT mice. Twenty-four hours after the administration, the lungs were removed and processed for β-gal staining. (B) Microscopic observation showed that SA β-gal-positive cells were found mainly in the bronchial epithelium, but also in some blood vessels and interstitial macrophages. (C) After the intratracheal administration of AdVASH1 to WT mice, the lungs were removed at the indicated time points; and tissue extracts prepared from them were then Western blotted for VASH1.
(TIFF)

Figure S4 VASH1 does not increase stress resistance of NHBECs. (A) Expression of endogenous VASH1 in HUVECs and NHBECs was analyzed by RT-PCR. (B) NHBECs were infected with AdVASH1 or AdLacZ. After a 72-hour incubation, Western blotting for VASH1, SOD2, and SIRT1 was performed. (C) NHBECs were infected with AdVASH1 or AdLacZ. After a 72-hour incubation, NHBECs were exposed to 400 μmol/L H_2O_2 for 24 hours; and the trypan blue exclusion assay was then performed. Blue-stained cells were quantified, and the % of dead cells was calculated. Values are the ratio of blue-stained cells to total cells, and are the means and SDs of 4 wells.
(TIFF)

Ackowledgments

We thank Ms. Yuriko Fujinoya for her excellent technical assistance.

Author Contributions

Conceived and designed the experiments: Y. Sato. Performed the experiments: HM TW HH. Analyzed the data: YH YO TK. Contributed reagents/materials/analysis tools: Y. Suzuki TN SI MO. Wrote the paper: HM TW Y. Sato.

References

1. Phng LK, Gerhardt H (2009) Angiogenesis: a team effort coordinated by notch. Dev Cell 16: 196–208.
2. Watanabe K, Hasegawa Y, Yamashita H, Shimizu K, Ding Y, et al. (2004) Vasohibin as an endothelium-derived negative feedback regulator of angiogenesis. J Clin Invest 114: 898–907.
3. Kimura H, Miyashita H, Suzuki Y, Kobayashi M, Watanabe K, et al. (2009) Distinctive localization and opposed roles of vasohibin-1 and vasohibin-2 in the regulation of angiogenesis. Blood 113: 4810–4818.
4. Andreassi MG (2009) Metabolic syndrome, diabetes and atherosclerosis: influence of gene-environment interaction. Mutat Res 667: 35–43.
5. Erusalimsky JD, Kurz DJ (2005) Cellular senescence in vivo: its relevance in ageing and cardiovascular disease. Exp Gerontol 40: 634–642.
6. Minamino T, Komuro I (2008) Role of telomeres in vascular senescence. Front Biosci 13: 2971–2979.
7. O'Riordan E, Mendelev N, Patschan S, Patschan D, Eskander J, et al. (2007) Chronic NOS inhibition actuates endothelial-mesenchymal transformation. Am J Physiol Heart Circ Physiol 292: H285–294.
8. Miyashita H, Suzuki H, Ohkuchi A, Sato Y (2011) Mutual Balance between Vasohibin-1 and Soluble VEGFR-1 in Endothelial Cells. Pharmaceuticals 4: 782–793.
9. Namba K, Abe M, Saito S, Satake M, Ohmoto T, et al. (2000) Indispensable role of the transcription factor PEBP2/CBF in angiogenic activity of a murine endothelial cell MSS31. Oncogene 19: 106–114.
10. Hosaka T, Kimura H, Heishi T, Suzuki Y, Miyashita H, et al. (2009) Vasohibin-1 expression in endothelium of tumor blood vessels regulates angiogenesis. Am J Pathol 175: 430–439.
11. Jang YC, Perez VI, Song W, Lustgarten MS, Salmon AB, et al. (2009) Overexpression of Mn superoxide dismutase does not increase life span in mice. J Gerontol A Biol Sci Med Sci 64: 1114–1125.
12. Yamashita H, Abe M, Watanabe K, Shimizu K, Moriya T, et al. (2006) Vasohibin prevents arterial neointimal formation through angiogenesis inhibition. Biochem Biophys Res Commun 345: 919–925.
13. DuPage M, Dooley AL, Jacks T (2009) Conditional mouse lung cancer models using adenoviral or lentiviral delivery of Cre recombinase. Nat Protoc 4: 1064–1072.
14. Zhan H, Suzuki T, Aizawa K, Miyagawa K, Nagai R (2010) Ataxia telangiectasia mutated (ATM)-mediated DNA damage response in oxidative stress-induced vascular endothelial cell senescence. J Biol Chem 285: 29662–29670.
15. Rajawat YS, Hilioti Z, Bossis I (2009) Aging: central role for autophagy and the lysosomal degradative system. Ageing Res Rev 8: 199–213.
16. Suzuki Y, Kobayashi M, Miyashita H, Ohta H, Sonoda H, et al. (2010) Isolation of a small vasohibin-binding protein (SVBP) and its role in vasohibin secretion. J Cell Sci 123: 3094–3101.
17. Hinman MN, Lou H (2008) Diverse molecular functions of Hu proteins. Cell Mol Life Sci 65: 3168–3181.
18. Abdelmohsen K, Lal A, Kim HH, Gorospe M (2007) Posttranscriptional orchestration of an anti-apoptotic program by HuR. Cell Cycle 6: 1288–1292.
19. Lee S, Chen TT, Barber CL, Jordan MC, Murdock J, et al. (2007) Autocrine VEGF signaling is required for vascular homeostasis. Cell 130: 691–703.
20. Bertram C, Hass R (2008) Cellular responses to reactive oxygen species-induced DNA damage and aging. Biol Chem 389: 211–220.
21. Potente M, Dimmeler S (2008) Emerging roles of SIRT1 in vascular endothelial homeostasis. Cell Cycle 7: 2117–22.
22. Gorospe M, de Cabo R (2008) AsSIRTing the DNA damage response. Trends Cell Biol 18: 77–83.
23. Tomita M, Okuyama T, Katsuyama H, Miura Y, Nishimura Y, et al. (2007) Mouse model of paraquat-poisoned lungs and its gene expression profile. Toxicology 231: 200–209.
24. Gurevich F, Perazella MA (2009) Renal effects of anti-angiogenesis therapy: update for the internist. Am J Med 122: 322–328.
25. Heishi T, Hosaka T, Suzuki Y, Miyashita H, Oike Y, et al. (2010) Endogenous angiogenesis inhibitor vasohibin1 exhibits broad-spectrum antilymphangiogenic activity and suppresses lymph node metastasis. Am J Pathol 176: 1950–1958.
26. Saito D, Maeshima Y, Nasu T, Yamasaki H, Tanabe K, et al. (2011) Amelioration of renal alterations in obese type 2 diabetic mice by vasohibin-1, a negative feedback regulator of angiogenesis. Am J Physiol Renal Physiol 300: F873–886.
27. Shimizu K, Watanabe K, Yamashita H, Abe M, Yoshimatsu H, et al. (2005) Gene regulation of a novel angiogenesis inhibitor, vasohibin, in endothelial cells. Biochem Biophys Res Commun 327: 700–706.
28. Ushio-Fukai M, Alexander RW (2004) Reactive oxygen species as mediators of angiogenesis signaling: role of NAD(P)H oxidase. Mol Cell Biochem 264: 85–97.
29. Fukai T, Ushio-Fukai M (2011) Superoxide dismutases: role in redox signaling, vascular function, and diseases. Antioxid Redox Signal. 15:1583–1606.
30. Suzuki K, Tatsumi H, Satoh S, Senda T, Nakata T, et al. (1993) Manganese-superoxide dismutase in endothelial cells: localization and mechanism of induction. Am J Physiol 265: H1173–1178.
31. Didion SP, Faraci FM (2005) Ceramide-induced impairment of endothelial function is prevented by CuZn superoxide dismutase overexpression. Arterioscler Thromb Vasc Biol 25: 90–95.
32. Finkel T, Deng CX, Mostoslavsky R (2009) Recent progress in the biology and physiology of sirtuins. Nature 460: 587–591.
33. Orimo M, Minamino T, Miyauchi H, Tateno K, Okada S, et al. (2009) Protective role of SIRT1 in diabetic vascular dysfunction. Arterioscler Thromb Vasc Biol 29: 889–894.
34. Stein S, Lohmann C, Schafer N, Hofmann J, Rohrer L, et al. (2010) SIRT1 decreases Lox-1-mediated foam cell formation in atherogenesis. Eur Heart J 31: 2301–2309.
35. Takemura A, Iijima K, Ota H, Son BK, Ito Y, et al. (2011) Sirtuin 1 retards hyperphosphatemia-induced calcification of vascular smooth muscle cells. Arterioscler Thromb Vasc Biol 31: 2054–2062.
36. Zhang QJ, Wang Z, Chen HZ, Zhou S, Zheng W, et al. (2008) Endothelium-specific overexpression of class III deacetylase SIRT1 decreases atherosclerosis in apolipoprotein E-deficient mice. Cardiovasc Res 80: 191–199.
37. Potente M, Ghaeni L, Baldessari D, Mostoslavsky R, Rossig L, et al. (2007) SIRT1 controls endothelial angiogenic functions during vascular growth. Genes Dev 21: 2644–2658.

38. Ono M (2008) Molecular links between tumor angiogenesis and inflammation: inflammatory stimuli of macrophages and cancer cells as targets for therapeutic strategy. Cancer Sci 99: 1501–1506.
39. Naik E, Dixit VM (2011) Mitochondrial reactive oxygen species drive proinflammatory cytokine production. J Exp Med 208: 417–420.
40. Shibuya T, Watanabe K, Yamashita H, Shimizu K, Miyashita H, et al. (2006) Isolation and characterization of vasohibin-2 as a homologue of VEGF-inducible endothelium-derived angiogenesis inhibitor vasohibin. Arterioscler Thromb Vasc Biol 26: 1051–1057.
41. Chen J, Patschan S, Goligorsky MS (2008) Stress-induced premature senescence of endothelial cells. J Nephrol 21: 337–344.
42. Nasu T, Maeshima Y, Kinomura M, Hirokoshi-Kawahara K, Tanabe K, et al. (2009) Vasohibin-1, a negative feedback regulator of angiogenesis, ameliorates renal alterations in a mouse model of diabetic nephropathy. Diabetes 58: 2365–2375.
43. Han MK (2011) Update in chronic obstructive pulmonary disease in 2010. Am J Respir Crit Care Med 183: 1311–1315.
44. Jerkic M, Kabir MG, Davies A, Yu LX, McIntyre BA, et al. (2011) Pulmonary hypertension in adult Alk1 heterozygous mice due to oxidative stress. Cardiovasc Res 92: 375–384.
45. de Perrot M, Liu M, Waddell TK, Keshavjee S (2003) Ischemia-reperfusion-induced lung injury. Am J Respir Crit Care Med 167: 490–511.
46. Nakamaru Y, Vuppusetty C, Wada H, Milne JC, Ito M, et al. (2009) A protein deacetylase SIRT1 is a negative regulator of metalloproteinase-9. FASEB J 23: 2810–2819.
47. Rajendrasozhan S, Yang SR, Kinnula VL, Rahman I (2008) SIRT1, an antiinflammatory and antiaging protein, is decreased in lungs of patients with chronic obstructive pulmonary disease. Am J Respir Crit Care Med. 177: 861–870.
48. Siedlinski M, van Diemen CC, Postma DS, Vonk JM, Boezen HM (2009) Superoxide dismutases, lung function and bronchial responsiveness in a general population. Eur Respir J 33: 986–992.

Vascular Pharmacology 56 (2012) 262–266

Contents lists available at SciVerse ScienceDirect

Vascular Pharmacology

journal homepage: www.elsevier.com/locate/vph

Review

The vasohibin family: Novel regulators of angiogenesis

Yasufumi Sato *

Department of Vascular Biology, Institute of Development, Aging and Cancer, Tohoku University, 4-1 Seiryo-machi, Aoba-ku, Sendai 980-8575, Japan

ARTICLE INFO

Article history:
Received 15 November 2011
Received in revised form 5 January 2012
Accepted 15 January 2012

Keywords:
Vasohibin
Angiogenesis

ABSTRACT

Angiogenesis is thought to be regulated by the local balance between angiogenesis stimulators and angiogenesis inhibitors. A number of endogenous regulators of angiogenesis have been found in the body. We recently isolated vasohibin-1 (VASH1) as a negative feedback regulator of angiogenesis produced by endothelial cells, and VASH2 as a homologue of VASH1 thereafter. We found that VASH1 was expressed in endothelial cells to terminate angiogenesis, whereas VASH2 promoted angiogenesis, in the mouse model of angiogenesis. This mini-review will focus on the vasohibin family in relation to the regulation of angiogenesis.

Contents

1. Introduction

The vasculature is primarily composed of luminal endothelial cells (ECs) and surrounding mural cells (smooth muscle cells or pericytes). ECs are multifunctional cells covering the entire luminal surface of all blood vessels. They form an interface between the circulating blood in the lumen and the rest of the vessel wall, and maintain vascular homeostasis. ECs control the transport of various molecules across the vascular wall, regulate the adhesion of leukocytes for extravasation, manipulate vascular tonus, and prevent thrombotic events. When stimulated by angiogenic factors, ECs form neo-vessels. The initial step of angiogenesis is the extrication of mural cells from the endothelial tubes for vascular destabilization. Subsequently, specialized ECs, the so-called "tip" cells, migrate by extending numerous filopodia, whereas the ECs that follow them, the so-called "stalk" cells, proliferate, causing elongation of the sprouts to form immature tube-like structures. Finally, redistributed mural cells affix themselves to the newly formed vessels for vascular restabilization. By this process, ECs stop their proliferation, thus terminating angiogenesis (Gerhardt and Betsholtz, 2003).

The body contains a number of endogenous angiogenesis stimulators and inhibitors, and the local balance between them regulates this process of blood vessel formation. Angiogenesis stimulators are mostly growth factors and cytokines including vascular endothelial growth factor (VEGF), whereas angiogenesis inhibitors are variable and include hormones, chemokines, proteins accumulated in the extracellular matrix, proteolytic fragments of various proteins, and so forth (Sato, 2006). In addition, the majority of angiogenesis inhibitors are extrinsic to the vasculature; however, some are constitutively expressed there and act as barriers to prevent the invasion by sprouts, and other factors are generated in response to certain stimuli and counteract this process. Recently, however, ECs themselves have been found to produce intrinsic angiogenesis inhibitors. Such inhibitors may regulate angiogenesis in an auto-regulatory or negative-feedback fashion.

2. Vasohibin-1 (VASH1)

We hypothesized that ECs themselves might produce either positive or negative regulators of angiogenesis. To test this hypothesis, we

* Tel.: +81 22 717 8528; fax: +81 22 717 8533.
E-mail address: y-sato@idac.tohoku.ac.jp.

1537-1891/$ – see front matter © 2012 Elsevier Inc. All rights reserved.
doi:10.1016/j.vph.2012.01.002

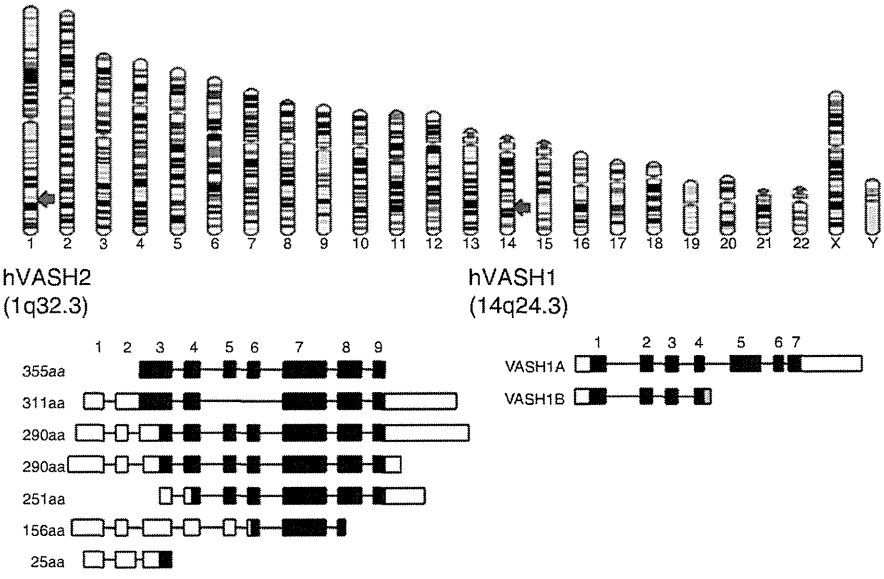

Fig. 1. *VASH1* and *VASH2* genes and their transcripts.The human *VASH1* gene is encoded in 14q24.3; and the human *VASH2* gene, in 1q32.3. There are multiple transcripts in both human VASH1 and VASH2. Black squares indicate the exons encoding the protein.

performed DNA microarray analysis to detect VEGF-inducible genes in ECs (Abe and Sato, 2001). Among a variety of VEGF-inducible genes, we focused our attention on those genes whose functions were undefined at that time. We performed *in vitro* functional assays for angiogenesis, isolated the molecule VASH1, and demonstrated its anti-angiogenic activity *in vivo* (Watanabe et al., 2004). The gene for human *VASH1* gene is located on chromosome 14q24.3, and consists of 7 exons (Fig. 1). There are 2 isoforms of human VASH1: full-length VASH1A and its spliced variant, VASH1B (Fig. 1). Human VASH1A protein is composed of 365 amino acid residues; whereas human VASH1B protein is composed of 204 amino acid residues, and this splicing variant also has the anti-angiogenic activity (Shimizu et al., 2005; Kern et al., 2008).

The VEGFR-induced expression of VASH1 in ECs is mediated via VEGFR2 and its downstream effector PKCδ (Shimizu et al., 2005). VASH1 is induced not only by VEGF but also by fibroblast growth factor 2 (FGF-2), another potent angiogenic factor (Watanabe et al., 2004; Shimizu et al., 2005); and this induction is also mediated by PKCδ (Shimizu et al., 2005). Accordingly, the principal signaling pathways for the induction of VASH1 by these 2 representative angiogenic growth factors considerably overlap. Interestingly, this induction of VASH1 in ECs disappears under a hypoxic condition or in the presence of inflammatory cytokines such as TNFα and IL-1 (Shimizu et al., 2005).

Immunohistochemical analysis revealed that VASH1 protein is present in ECs in the developing human or mouse embryo, but is reduced in expression in the post-neonate (Shibuya et al., 2006). Nimmagadda et al. independently showed by *in situ* hybridization that VASH1 mRNA is expressed in a wide range of tissues and organs in the chicken embryo, and suggested that the expression of VASH1 might not be limited to ECs (Nimmagadda et al., 2007). Indeed, we could detect VASH1 mRNA in hematopoietic stem cells in the bone marrow (Naito et al., 2009). Nevertheless, our immunohistochemical analysis preferentially detected VASH1 protein in ECs at the site of angiogenesis (Watanabe et al., 2004; Shibuya et al., 2006). We further investigated the expression of VASH1 under various conditions giving rise to pathological angiogenesis. The presence of VASH1 in ECs is evident in various cancers, atherosclerotic lesions, age-dependent macular degeneration (AMD), diabetic retinopathy, and rheumatoid arthritis (Yamashita et al., 2006; Yoshinaga et al., 2008; Wakusawa et al., 2008; Tamaki et al., 2008; Sato et al., 2009; Hosaka et al., 2009; Miyake et al., 2009; Tamaki et al., 2010; Yoshinaga et al., 2011). Even under these pathological conditions, the extent of angiogenesis may vary in its natural course. Interestingly, patients with active AMD tend to have a lower VASH1-to-VEGF mRNA ratio than those with the inactive disease (Wakusawa et al., 2008). Tumors inoculated into *VASH1 (−/−)* mice contain numerous immature vessels, resulting in a growth advantage to the tumors (Hosaka et al., 2009). These observations suggest that VASH1 may regulate the course of angiogenesis under pathological conditions as well.

Peripheral lymphatic vessels are composed of a single layer of lymphatic ECs without mural cell coverage, and their function is to collect fluid lost from blood vessels and to maintain immune responses, lipid uptake, and tissue homeostasis. Recently, attention has been focused on lymphangiogenesis, which is the formation of new lymphatic vessels; because it has been shown to be related to the lymph node (LN) metastasis of cancers. Angiogenesis is counter-balanced by various endogenous inhibitors. However, little is known about endogenous inhibitors of lymphangiogenesis. We reevaluated the effect of VASH1 by using the corneal micropocket assay, and observed its broad-spectrum anti-angiogenic as well as anti-lymphangiogenic activities (Heishi et al., 2010). In addition, we found that VASH1 inhibits tumor lymphangiogenesis and tumor LN metastasis (Heishi et al., 2010). To our knowledge, VASH1 is the first molecule intrinsic to the endothelium that exhibits anti-lymphangiogenic activities.

3. Vasohibin-2 (VASH2)

By database searching, we found 1 gene homologous to *VASH1*, and designated it as *VASH2* (Nimmagadda et al., 2007). The gene for human *VASH2* is located on chromosome 1q32.3. So far, the 9 exons for the *VASH2* gene have been shown in the database to form multiple transcripts owing to alternative splicing (Fig. 1). We found that full-length human VASH2, composed of 355 amino acid residues, was expressed in cultured ECs (Nimmagadda et al., 2007). The expression of VASH2 seems to be constitutive and cannot be induced by any growth factors or cytokines.

Because of the similarity between VASH1 and VASH2, we examined their spatiotemporal expression and function during angiogenesis (Kimura et al., 2009). Our analysis using the mouse subcutaneous angiogenesis model revealed that VASH1 is expressed not in ECs at the sprouting front but in newly formed blood vessels behind the sprouting front where angiogenesis is terminated. In contrast, VASH2

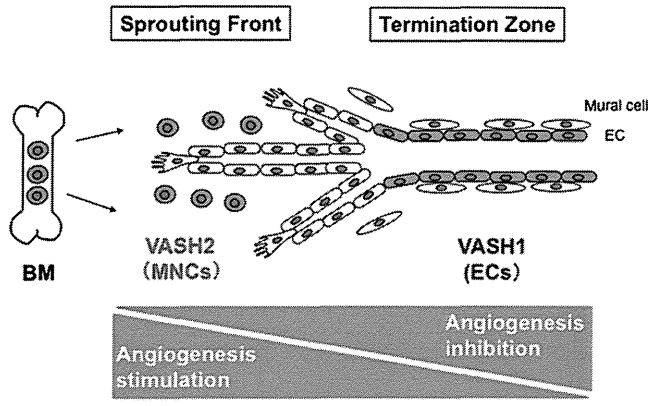

Fig. 2. Spatial expression and function of VASH1 and VASH2 in the regulation of angiogenesis.VASH1 is mainly expressed in ECs at the termination zone and halts angiogenesis. In contrast, VASH2 is mainly expressed in MNCs at the sprouting front and promotes angiogenesis. BM: bone marrow.

is expressed preferentially in mononuclear cells (MNCs) that are mobilized from the bone marrow and infiltrate the sprouting front. We then generated VASH1 and VASH2 knockout mice. *VASH1 KO* mice contain numerous immature microvessels in the area where angiogenesis should be terminated. This phenotype is gene-dosage sensitive, as angiogenesis is greater in *VASH1 (−/−)* mice than in *VASH1 (+/−)* ones (Kimura et al., 2009). Importantly, newly formed immature microvessels in *VASH1 (−/−)* mice are functional, as indicated by blood flow (Kimura et al., 2009). In contrast, *VASH2 KO* mice contain fewer neovessels in the sprouting front of angiogenesis. This phenotype is also gene-dosage sensitive, as more impaired angiogenesis is observed in the *VASH2 (−/−)* mice (Kimura et al., 2009). Importantly, the degree of infiltration of the sprouting front by MNCs in *VASH2 (−/−)* mice is identical to that in wild-type mice (Kimura et al., 2009). As stated above, the expression of VASH1 is low in proliferating ECs at the sprouting front, but is high in non-proliferating ECs (Kimura et al., 2009). In addition, angiogenesis in the *VASH2* knockout mice is deficient at the sprouting front (Kimura et al., 2009). These results indicate that VASH1 is expressed in ECs in the termination zone of angiogenesis to terminate angiogenesis and that VASH2 is mainly expressed in MNCs in the sprouting front and promotes angiogenesis (Fig. 2).

4. Small vasohibin-binding protein (SVBP)

To disclose the undefined characteristics of vasohibins, we searched for their possible binding partners by using the yeast two-hybrid technique and discovered 1 candidate gene (Suzuki et al., 2010). This gene has been registered as hypothetical protein LOC374969 or coiled-coil domain containing 23. We confirmed the binding of this protein to VASH1 and VASH2 by using the BIAcore system (Fig. 3). Since this protein is composed of only 66 amino acids, we renamed it as SVBP (Suzuki et al., 2010). A database search revealed that SVBP is highly conserved among species (Fig. 3). We then examined the function of SVBP and found that this small molecule binds to vasohibins within the cell, forming a hetero-complex and facilitating the secretion of vasohibin from the cell. As vasohibins lack the classical signal sequence for secretion, it has been unclear whether vasohibins are indeed secreted (Suzuki et al., 2010). We therefore propose that SVBP functions as a secretory chaperone of vasohibins.

5. Bioinformatics of VASH1 and VASH2

The overall homology between full-length human VASH1 and VASH2 is 52.5% at the amino acid level. We conducted a database search on VASH1 and VASH2 of different species and discovered that the sea squirt possesses 1 common ancestral vasohibin gene and that the homology between this ancestral gene and human VASH1 or human VASH2 is almost the same. All vertebrates have VASH1 and VASH2. Thus, this common ancestral gene seems to be have divided into VASH1 and VASH2 during the evolution to vertebrate. Amino acid sequences of mammalian VASH1 and VASH2 are well conserved among species, and this trend is more noticeable for VASH2 (Fig. 4).

We searched for known functional motifs in the amino acid sequences, but we could not find any in either VASH1 or VASH2, making it extremely difficult to estimate and compare the functions or three-dimensional structures of these 2 molecules. We therefore surveyed the order/disorder orientation of VASH1 and VASH2 proteins. The order region defines stability in a three-dimensional composition whereas the disorder region defines instability in it. As shown in Fig. 5, VASH1 and VASH2 contain disorder regions (in red type) in both N-terminus and C-terminus ends, with order regions (in black type) in the middle part of their structure. The overall order/disorder probability lines of VASH1 and VASH2 considerably resemble each

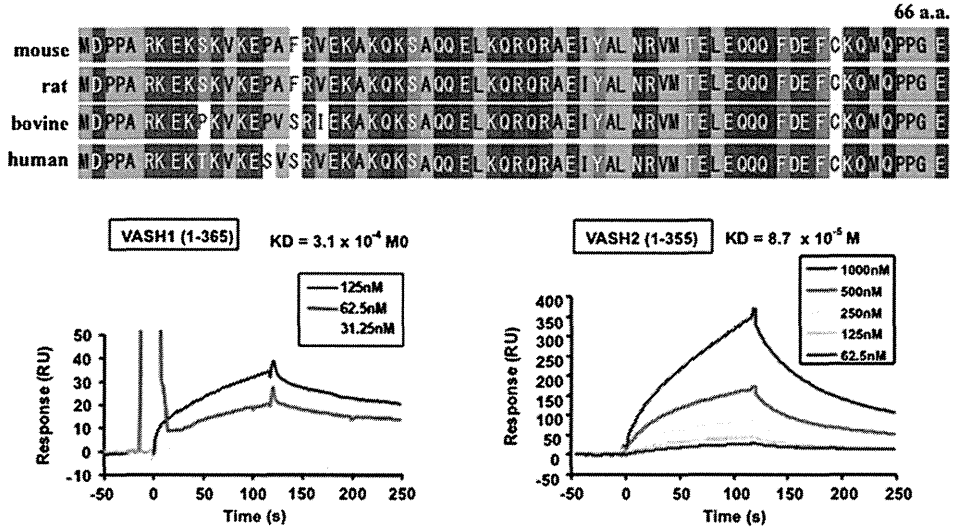

Fig. 3. SVBP of various species and its binding to VASH1/VASH2.Amino acid sequences of SVBP from the indicated species are shown in the upper panel. Binding characteristics of SVAB and VASH1/VASH2 are seen in the lower panel.

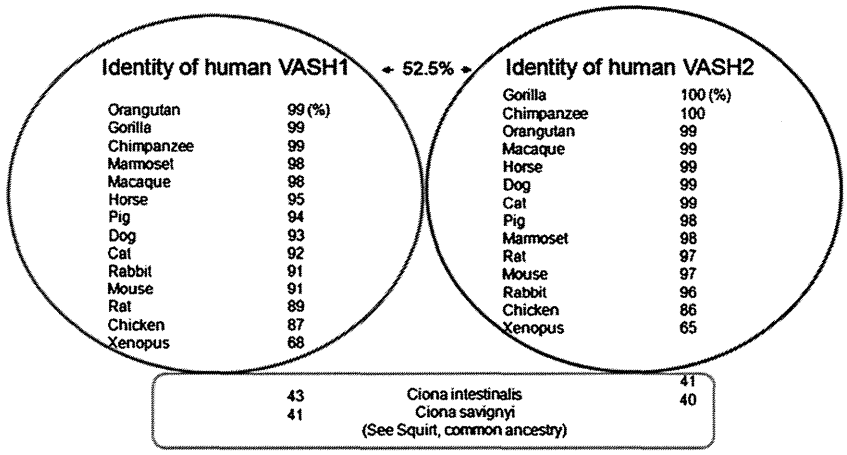

Fig. 4. Vasohibin family proteins of various species.Similarities of vasohibin family proteins of various species are shown. Proteins within the red circle are VASH1; and those within the blue circle, VASH2. Proteins within the green rectangle are ancestral gene products.

other, indicating the correspondence of these 2 molecules. However, when the similarity of order and disorder areas of the VASH's is compared, the resemblance in the disorder areas is less (Fig. 5). As it has been recently noted, the disorder region is more important than the order one for determining the function of proteins (Uversky, 2011). Therefore, differences in the disorder regions may indicate the distinctive function of VASH1 and VASH2.

6. Concluding remarks

The present mini-review has focused on the novel VASH family of proteins, VASH1 and VASH2. VASH1 and VASH2 are highly conserved among species. However, the lack of any known functional motifs makes it extremely difficult to estimate and compare the functions or three-dimensional structures of VASH1 and VAH2. Nevertheless, our analysis indicates that their roles in the regulation of angiogenesis are distinct and perhaps contradictory.

We are now characterizing their receptor and its downstream signaling. We hope that our work will disclose the entire function of this unique family of proteins.

Acknowledgements

I thank Professor Kengo Kinoshita at Department of Applied Information Sciences, Graduate School of Information Sciences, Tohoku University for a fruitful discussion.

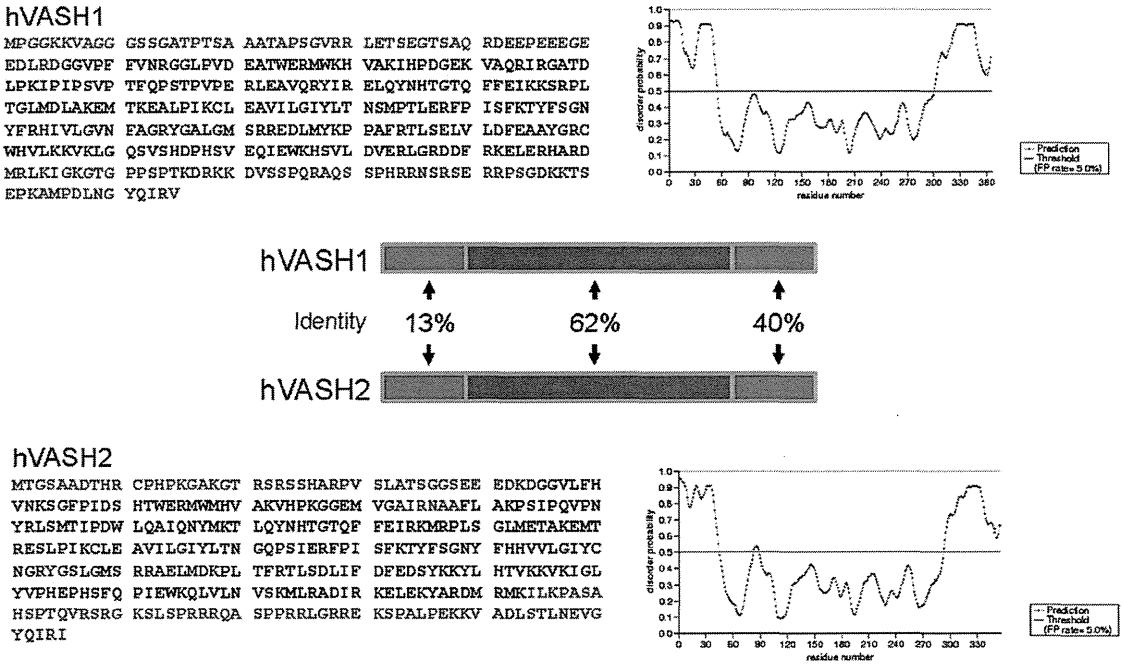

Fig. 5. Order/disorder configuration of human VASH1 and VASH2.Order/disorder configuration was determined by the Protein Disorder Prediction System (http://prdos.hgc.jp/cgi-bin/top.cgi). Amino acid sequences of human VASH1 and human VASH2 are shown on the left. Areas of red letters indicate disorder regions, whereas areas of black ones indicate the order region. The lines of disorder probability are shown graphically at the right. The similarity of order and disorder regions is indicated in the center.

References

Gerhardt, H., Betsholtz, C., 2003. Endothelial-pericyte interactions in angiogenesis. Cell Tissue Res. 314, 15–23.

Sato, Y., 2006. Update on endogenous inhibitors of angiogenesis. Endothelium 13, 147–155.

Abe, M., Sato, Y., 2001. cDNA microarray analysis of the gene expression profile of VEGF-induced human umbilical vein endothelial cells. Angiogenesis 4, 289–298.

Watanabe, K., et al., 2004. Vasohibin as an endothelium-derived negative feedback regulator of angiogenesis. J. Clin. Invest. 114, 898–907.

Shimizu, K., et al., 2005. Gene regulation of a novel angiogenesis inhibitor, vasohibin, in endothelial cells. Biochem. Biophys. Res. Commun. 327, 700–706.

Kern, J., et al., 2008. Alternative splicing of vasohibin-1 generates an inhibitor of endothelial cell proliferation, migration, and capillary tube formation. Arterioscler. Thromb. Vasc. Biol. 28, 478–484.

Shibuya, T., et al., 2006. Isolation and characterization of vasohibin-2 as a homologue of VEGF-inducible endothelium-derived angiogenesis inhibitor vasohibin. Arterioscler. Thromb. Vasc. Biol. 26, 1051–1057.

Nimmagadda, S., et al., 2007. Expression pattern of vasohibin during chick development. Dev. Dyn. 236, 1358–1362.

Naito, H., et al., 2009. Induction and expression of anti-angiogenic vasohibins in the hematopoietic stem/progenitor cell population. J. Biochem. 145, 653–659.

Yamashita, H., et al., 2006. Vasohibin prevents arterial neointimal formation through angiogenesis inhibition. Biochem. Biophys. Res. Commun. 345, 919–925.

Yoshinaga, K., et al., 2008. Expression of vasohibin as a novel endothelium-derived angiogenesis inhibitor in endometrial cancer. Cancer Sci. 99, 914–919.

Wakusawa, R., et al., 2008. Expression of vasohibin, an antiangiogenic factor, in human choroidal neovascular membranes. Am. J. Ophthalmol. 146, 235–243.

Tamaki, K., et al., 2008. Vasohibin-1 in human breast carcinoma: a potential negative feedback regulator of angiogenesis. Cancer Sci. 100, 88–94.

Sato, H., et al., 2009. Vitreous levels of vasohibin-1 and vascular endothelial growth factor in patients with proliferative diabetic retinopathy. Diabetologia 52, 359–361.

Hosaka, T., et al., 2009. Vasohibin-1 expressed in endothelium of tumor vessels regulates angiogenesis. Am. J. Pathol. 175, 430–439.

Miyake, K., et al., 2009. Inflammatory cytokine-induced expression of vasohibin-1 by rheumatoid synovial fibroblasts. Acta Med. Okayama. 63, 349–358.

Tamaki, K., et al., 2010. Vasohibin-1 as a potential predictor of aggressive behavior of ductal carcinoma in situ of the breast. Cancer Sci. 101, 1051–1058.

Yoshinaga, K., et al., 2011. Roles of intrinsic angiogenesis inhibitor, vasohibin, in cervical carcinomas. Cancer Sci. 102, 446–451.

Heishi, T., et al., 2010. Endogenous angiogenesis inhibitor vasohibin1 exhibits a broad-spectrum anti-lymphangiogenic activity and suppresses lymph node metastasis. Am. J. Pathol. 176, 1950–1958.

Kimura, H., et al., 2009. Distinctive localization and opposed roles of vasohibin-1 and vasohibin-2 in the regulation of angiogenesis. Blood. 113, 4810–4818.

Suzuki, Y., et al., 2010. Isolation of a small vasohibin-binding protein (SVBP) and its role in vasohibin secretion. J. Cell Sci. 123, 3094–4101.

Uversky, V.N., 2011. Intrinsically disordered proteins from A to Z. Int. J. Biochem. Cell Biol. 43, 1090–1103.

The American Journal of Pathology, Vol. 180, No. 3, March 2012

DOI: 10.1016/j.ajpath.2011.11.008

Vascular Biology, Atherosclerosis, and Endothelium Biology

Promotion of Lymphatic Integrity by Angiopoietin-1/Tie2 Signaling during Inflammation

Kentaro Kajiya,* Hiroyasu Kidoya,† Mika Sawane,* Yuuko Matsumoto-Okazaki,* Haruyo Yamanishi,* Mikio Furuse,‡ and Nobuyuki Takakura†

From the Shiseido Innovative Science Research Center, Yokohama; the Department of Signal Transduction,† Research Institute of Microbial Diseases, Osaka University, Osaka; and the Department of Physiology and Cell Biology,‡ Kobe University, Kobe, Japan*

The cutaneous lymphatic system plays a major role in tissue fluid homeostasis and inflammation of the skin. Although several lymphangiogenic factors are known to be involved in the formation of lymphatic vessels, the molecular mechanisms that maintain lymphatic integrity and control the functional drainage of interstitial fluid and resolution of inflammation remain unknown. Here we show that angiopoietin-1 (Ang1) enhances lymphatic integrity and function during inflammation. Ang1 transgenic mice under the control of keratin-14 (K14-Ang1) showed attenuated edema formation and inflammation after UV B (UVB) exposure. After UVB irradiation, blood vascular permeability was inhibited in K14-Ang1 mice compared with wild-type (WT) mice. Moreover, lymphatic vessels of WT mice were markedly enlarged and leaky in inflamed skin, whereas K14-Ang1 mice showed relatively contracted lymphatic vessels together with enhanced lymphatic vascularization. Expression of endothelial-specific tight junction molecules claudin-5 and zonula occludens protein 1 (ZO-1) was strongly down-regulated in the inflamed lymphatic vessels of UVB-exposed WT mice, whereas down-regulation of both claudin-5 and ZO-1 was blocked in UVB-exposed K14-Ang1 mice. *In vitro* studies revealed that the stability of lymphatic endothelial cells was enhanced in the presence of Ang1, presumably via up-regulation of claudin-5, as well as ZO-1. Claudin-5 knockdown markedly increased the permeability of lymphatic endothelial cells. Overall, our data strongly support the idea that Ang1/Tie2 signaling promotes lymphatic integrity by modulating tight junction molecule expression during inflammation. ***(Am J Pathol 2012, 180:1273–1282; DOI: 10.1016/j.ajpath.2011.11.008)***

The lymphatic vascular system, which is composed of a dense network of thin-walled capillaries in peripheral tissues such as skin, plays a major role in the maintenance of tissue fluid homeostasis, and its impairment leads to lymphedema.[1,2] Another important aspect of lymphatic function is the afferent phase of immune response. Because lymphatic vessels are the conduit not only for excess water and macromolecules, but also for inflammatory cells such as macrophages, a detailed understanding of lymphatic function could lead to the development of methods to improve the resolution of inflammation. Indeed, recent findings in mouse models have indicated that the lymphatic vasculature is actively involved in inflammatory processes.[2–4]

Several lymphangiogenic factors, including vascular endothelial growth factor (VEGF)-C/-D/-A, platelet-derived growth factor–BB, angiopoietins, and hepatocyte growth factor (HGF), are known.[1,5] It has been shown that inflammation is attenuated in VEGF-C transgenic mice, or by subcutaneous delivery of VEGF-C, as a result of skin lymphangiogenesis, which promotes lymphatic function.[4,6] In contrast, adenoviral or transgenic delivery of VEGF-A induced the appearance of giant and functionally abnormal lymphatic vessels.[7] Systematic blockade of VEGF-A markedly reduced cutaneous photosensitivity and inflammation through inhibition of the enlargement of lymphatic vessels.[8] We also found that leaky and hyperpermeable inflamed lymphatics were associated with up-regulation of VEGF-A as well as down-regulation of VEGF-C.[6,8] Together, these data suggest that lymphangiogenic factors are actively involved in inflammation by mediating structural alteration of the lymphatics. Thus, application of other lymphangiogenic factors, which may directly regulate and/or cooperatively induce functional lymphangiogenesis in inflamed tissue, may have potential as a new strategy to accelerate the resolution of inflammation.

It recently was established that angiopoietin-1 (Ang1) promotes lymphatic vessel formation.[9,10] However, in

Accepted for publication November 14, 2011.

K.K. and H.K. contributed equally to this work.

Address reprint requests to Kentaro Kajiya, Ph.D., Shiseido Innovative Science Research Center, 2-12-1 Fukuura Kanazawa-ku, Yokohama 236-8643, Japan. E-mail: kentaro.kajiya@to.shiseido.co.jp.

contrast to the detailed understanding of the role of Ang1/Tie2 signaling in migration, permeability, and inflammation of blood vascular endothelial cells,[11] it remains unknown how lymphatic function is regulated by Ang1/Tie2 signaling. Structurally, lymphatic endothelial cells possess finely arranged, but unusual and discontinuous, junctions, consisting of adherens junctions, endothelial adhesion molecules, and tight junction proteins (TJPs) such as claudins, which allow the recirculation of fluid and cells transported to peripheral tissues via blood vessels.[12] It has been reported that claudin-5 knockout mice have increased permeability of the blood-brain barrier,[13] but the role of claudin-5 in lymphatic function is completely unknown. Here, we investigated how lymphatic function is modulated in angiopoietin-1 transgenic mice under the control of keratin 14 (K14-Ang1), to obtain insight into the molecular regulation of inflammation. Our results indicate that it may be feasible to treat edema and inflammation by the induction of functional lymphangiogenesis with Ang1.

Materials and Methods

Animals

Ten female WT mice and 10 K14-Ang1 transgenic mice[14] (kindly provided by Dr. George Yanconpoulous) at 8 to 15 weeks of age were exposed to a single dose of 200 mJ/cm^2 UV B (UVB) irradiation, using 10 Toshiba FL-20 SE fluorescent lamps (Toshiba, Tokyo, Japan) that deliver energy in the UVB wavelength range (280 to 340 nm, with a maximum at 305 nm).[15] Ten female WT and 10 K14-Ang1 mice without UVB irradiation also were used as controls. The thickness of the ears was measured every day until day 3 after irradiation. Three days after the UVB irradiation, the ears were removed, embedded in OCT compound, and processed for histologic analyses. All procedures, including measurement of ear thickness and UVB irradiation, were performed under anesthesia. All animal studies were approved by the Shiseido Research Center Committee on Research Animal Care.

Plasma Extravasation and Intravital Lymphangiography

To determine the blood vascular permeability, a Miles assay was performed as previously described.[16] Briefly, mice were anesthetized and intravenously injected with 150 μL of a 1% solution of Evans Blue dye in 0.9% NaCl. At 40 minutes after the dye injection, pictures of the ears were taken and the ears were removed. The dye was eluted from the dissected samples with formamide at 56°C, and the optical density was measured by spectrophotometry (Biotrak II; GE Healthcare, Fairfield, CT) at 620 nm. An intravital lymphatic permeability assay was conducted as described.[8] A 1-μL aliquot of a 1% solution of Evans Blue dye was injected intradermally at the inner surface of the rim of the ear, using a 10-μL Hamilton syringe, to visualize lymphatic vessels. The ear was photographed at 1, 5, and 10 minutes after dye injection.

Immunostaining

Immunofluorescence analysis was performed on 6-μm cryostat sections of mouse skins, using rat monoclonal antibodies against mouse LYVE-1 (MBL, Nagoya, Japan), against mouse Ki-67 antigen (DAKO Cytomation, Glostrup, Denmark), against mouse CD11b (BD Bioscience, Bedford, CA), and against mouse panendothelial cell antigen (clone: MECA-32; BD Bioscience), a hamster monoclonal antibody against mouse podoplanin (Angiobio, Del Mar, CA), and polyclonal antibodies against mouse LYVE-1 (RELIA Tech, Wolfenbuttel, Germany), against human claudin-5 (Santa Cruz Biotechnology, Santa Cruz, CA), against human zonula occludens protein 1 (ZO-1) (Invitrogen, Carlsbad, CA), and against mouse Prox1 (Covance, Emeryville, CA). Corresponding secondary antibodies labeled with AlexaFluor488 or AlexaFluor594 (Molecular Probes, Eugene, OR) were used. Routine H&E staining also was performed. Sections were examined with an Olympus AX80T microscope (Olympus, Tokyo, Japan) and images were captured with a DP controller digital camera (Olympus). Whole-ear skin was stained with monoclonal antibodies against CD31 (clone: MEC-13.3; BD Bioscience) and against podoplanin (Angiobio) and a polyclonal antibody against claudin-5 (Santa Cruz Biotechnology). Confocal microscopic examination of whole skin was performed using a LSM5 (Carl Zeiss, Thornwood, NY), and images were processed further using IMARIS (Carl Zeiss). Morphometric analyses were performed using IP-LAB software (Snanalytics, Fairfax, VA) as described.[17] Three different fields of each section were examined and the number of vessels per square micrometer, the average vessel size, and the relative tissue area occupied by lymphatic vessels were determined in an area of the dermis within a 200-μm distance from the epidermal-dermal junction. The unpaired Student's *t*-test was used to analyze differences in microvessel density and size.

Cells

Human dermal lymphatic endothelial cells (LECs) were isolated from neonatal human foreskins by immunomagnetic purification as described.[18] Lineage-specific differentiation was confirmed by means of real-time RT-PCR for the lymphatic vascular markers Prox1, LYVE-1, and podoplanin, and for the blood vascular endothelial markers VEGF receptor-1 and VEGF-C, as well as by immunostaining for CD31, Prox1, and podoplanin as described.[19] Cells were cultured in endothelial basal medium (EBM) 2 (Lonza, Basel, Switzerland) with supplements, for up to 11 passages.

Immunoblotting and Quantitative Real-Time RT-PCR

Western blot analyses of Tie1, Tie2, ZO-1, and claudin-5 were performed as described.[19] Briefly, confluent LECs were homogenized in lysis buffer, and protein concentrations were determined using the BCA-Kit (Pierce Biotech-

nology, Rockford, IL). LECs also were treated with 500 ng/mL Ang1 for 4 hours for the detection of claudin-5 and ZO-1, or for 10 minutes for the detection of phosphorylated Tie2 and Tie2. Equal amounts of lysates (100 μg protein) were immunoprecipitated with a rabbit polyclonal antibody against Tie1 or Tie2 (Santa Cruz Biotechnology) and then immunoblotted with a rabbit polyclonal antibody against Tie1, Tie2 (Santa Cruz Biotechnology), or phospho-Tie2 (Cell Signaling, Danvers, MA). In other experiments, equal amounts of lysates (5 μg protein) were immunoblotted with rabbit polyclonal antibody against Tie1, Tie2, claudin-5 (Santa Cruz Biotechnology), or ZO-1 (Invitrogen). Specific binding was detected by means of the enhanced chemiluminescence system (Amersham Biosciences, Piscataway, NJ). Equal loading was confirmed with an antibody against β-actin (Sigma, St. Louis, MO). In addition, total RNA was isolated from LECs cultured in the presence or absence of Ang1 (10 to 100 ng) for 4 hours after serum starvation. The expression of claudin-5 mRNA was examined by quantitative real-time RT-PCR, using the ABI Prism 7000 Sequence Detection System (Applied Biosystems, Foster City, CA). The probes and primers for claudin-5 and Tie2 were predesigned by Applied Biosystems (assay IDs: Hs00533949_m1 and Hs00176096_m1, respectively). Expression levels were normalized with respect to β-actin as an internal control (forward primer: 5′-TCACCGAGCGCGGCT-3′, reverse primer: 5′-TAATGTCACGCACGATTTCCC-3′) and probe (5′-FAM-CAGCTTCACCACCACGGCCGAG -TAMRA-3′).

siRNA Transfection

Small interfering RNA (siRNA) transfection was performed using the Basic Nucleofactor Kit for primary mammalian endothelial cells (Amaxa Biosystems, Cologne, Germany) as described.[20] Briefly, after trypsinization, LECs (5×10^5) were resuspended in 100 μL of basic nucleofactor solution. Cells were transfected by electroporation (Nucleofactor II; Amaxa Biosystems), using 2.0 μg siRNA containing two different double-stranded oligonucleotides for Tie1, Tie2, claudin-5, or control siRNA. The following siRNAs were used: Tie2: 5′-GGUGCCAUGGACUUGAUCUdTdT-3′ and 5′-GGCUAGUAAGAUCAAUGGUdTdT-3′, Tie1: 5′-GGUGACACCGCUGUACUUUdTdT-3′ and 5′-GGUUACUUGUAUAUCGCUAdTdT-3′, claudin-5: 5′-GGCUAAGAAUCUGCUUAGUdTdT-3′ and 5′-CGGAAUGAAGUUUCCUUUU-3′. Control siRNA (silencer negative control #1 siRNA; Ambion, Cambridgeshire, UK) comprised a 19-bp scrambled sequence with 3′dT overhangs, having no significant sequence homology to any known gene sequence. At 72 hours after transfection, cells were used for immunoblotting or assays. Efficient knockdown of these genes was confirmed by immunoblotting.

Migration, Cord Formation, and Permeability Assays

Haptotactic cell migration of LECs was studied as described,[19] using 24-well FluoroBlok inserts of 8-μm pore size (Falcon, Franklin Lakes, NJ). Briefly, the bottom sides of the inserts were coated with 10 μg/mL fibronec-

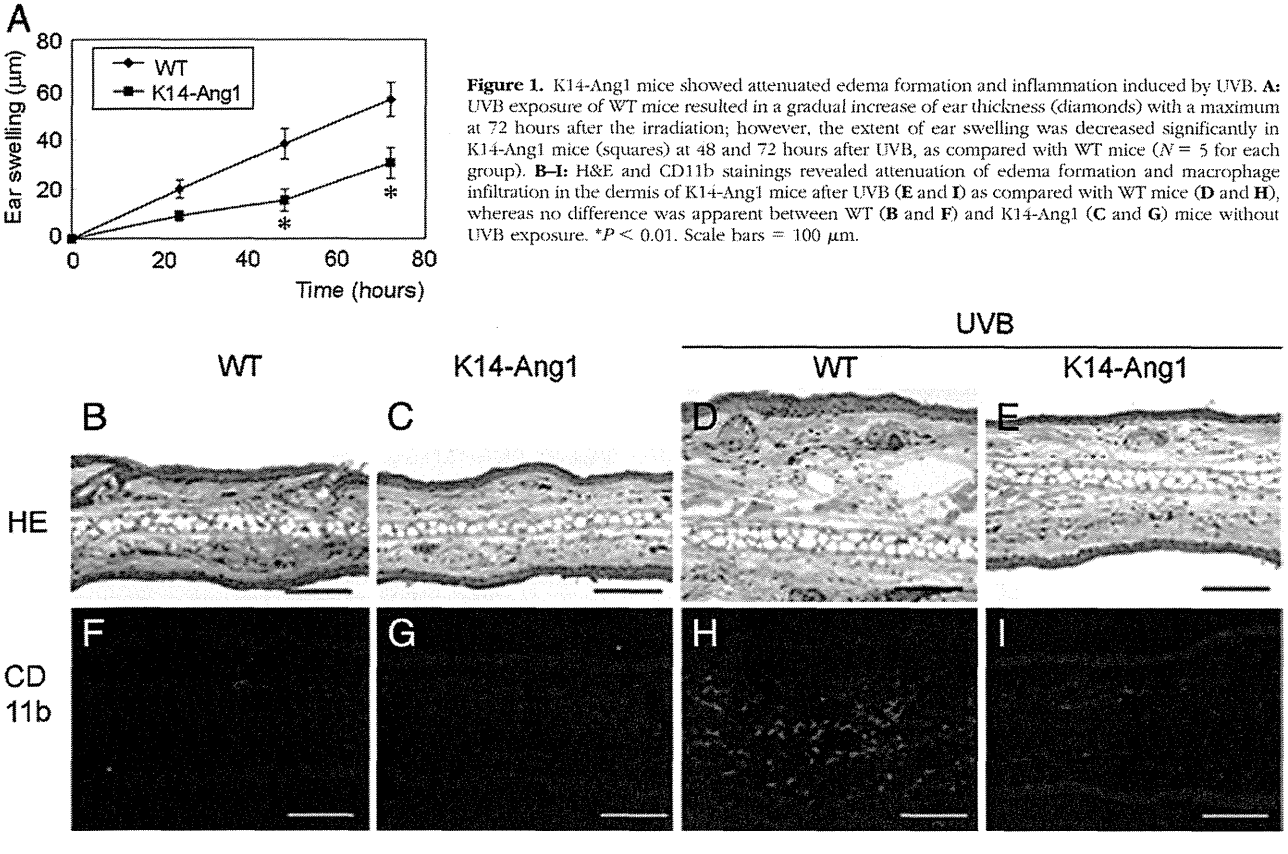

Figure 1. K14-Ang1 mice showed attenuated edema formation and inflammation induced by UVB. **A:** UVB exposure of WT mice resulted in a gradual increase of ear thickness (diamonds) with a maximum at 72 hours after the irradiation; however, the extent of ear swelling was decreased significantly in K14-Ang1 mice (squares) at 48 and 72 hours after UVB, as compared with WT mice ($N = 5$ for each group). **B–I:** H&E and CD11b stainings revealed attenuation of edema formation and macrophage infiltration in the dermis of K14-Ang1 mice after UVB (**E** and **I**) as compared with WT mice (**D** and **H**), whereas no difference was apparent between WT (**B** and **F**) and K14-Ang1 (**C** and **G**) mice without UVB exposure. $^*P < 0.01$. Scale bars = 100 μm.

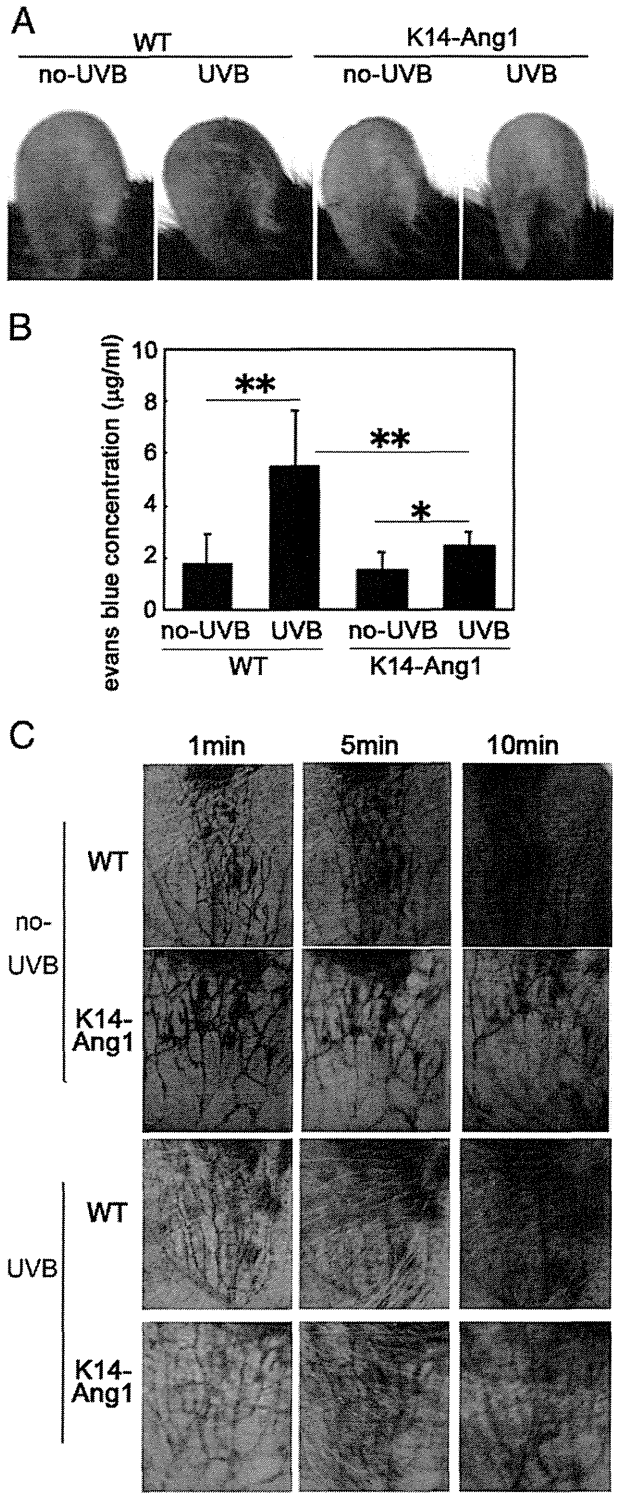

Figure 2. Decreased hyperpermeability of blood vessels as well as lymphatic vessels in K14-Ang1 mice during inflammation. **A:** The Miles assay revealed that UVB exposure induced vascular hyperpermeability of WT mice, whereas this effect was inhibited markedly in K14-Ang1 mice, as compared with WT. **B:** Quantitative analysis showed increased Evans blue leakage in the ear of UVB-irradiated WT mice as compared with UVB-irradiated K14-Ang1 mice ($N = 3$ for each group). **C:** Intravital lymphangiography revealed that lymph leakage was apparent in the whole ear of UVB-exposed WT mice at 5 and 10 minutes after dye injection, whereas the leakage was attenuated markedly in K14-Ang1 mice as compared with WT. Without UVB, there was no significant difference of lymph leakage at 5 minutes, however, at 10 minutes K14-Ang1 mice showed inhibited dye leakage. $^{*}P < 0.05$, $^{**}P < 0.01$.

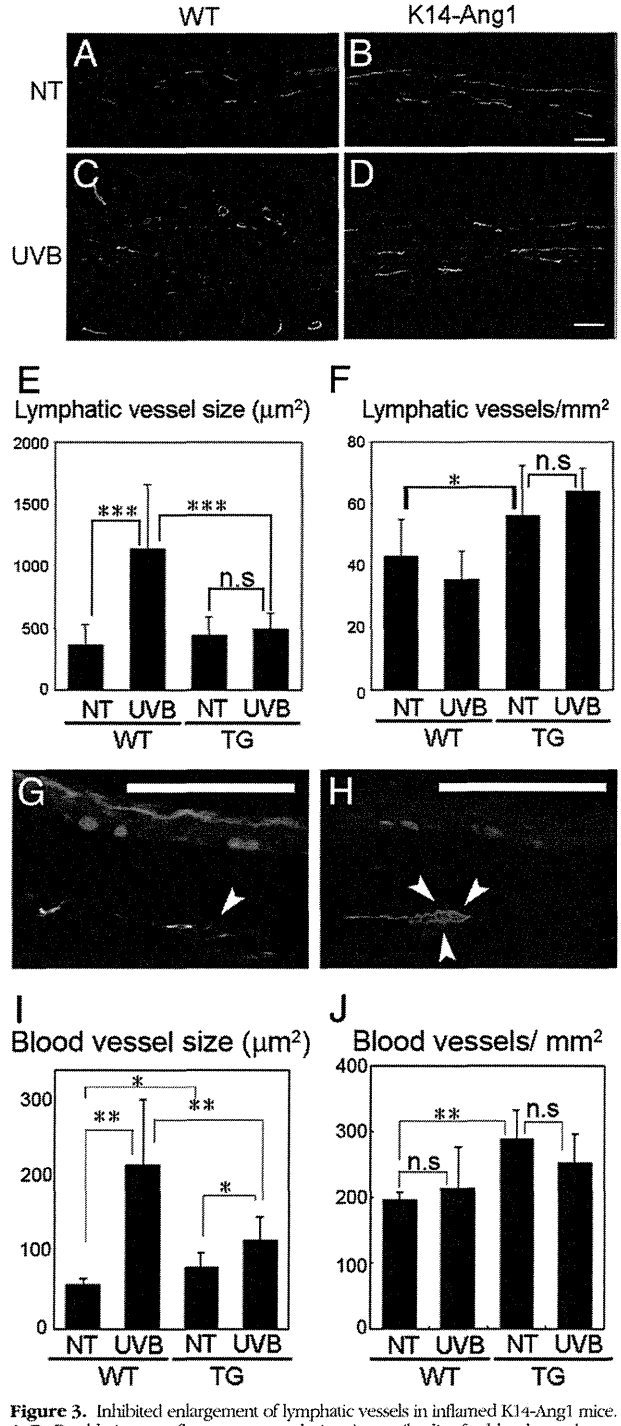

Figure 3. Inhibited enlargement of lymphatic vessels in inflamed K14-Ang1 mice. **A–D:** Double-immunofluorescence analysis using antibodies for blood vessel–specific antigen, panendothelial antigen-1 (red), and LYVE-1 (green) revealed marked enlargement of LYVE-1–positive lymphatic vessels in UVB-exposed WT mice (**C**) as compared with ear skin not exposed to UVB (non-UV) (**A**), whereas in K14-Ang1 mice, the enlargement of lymphatic vessels after UVB exposure was attenuated (**D**). In contrast, more lymphatic vessels were found in K14-Ang1 mice (**B**), as compared with WT mice (**D**). **E** and **F:** Morphometric analysis using ear sections stained with LYVE-1 showed pronounced enlargement of lymphatic vessels of WT mice after UVB irradiation, whereas the lymphatic enlargement was strongly inhibited in K14-Ang1 mice (**E**). The density of lymphatic vessels was increased in K14-Ang1 mice, as compared with WT mice (**F**). **G** and **H:** Double-immunofluorescence analysis for proliferation marker Ki-67 (red) and podoplanin (green) showed greater proliferation of lymphatic endothelial cells in K14-Ang1 mice (**H, arrowheads**) as compared with WT mice (**G, arrowheads**). **I** and **J:** Under physiological conditions, the size (**I**) and density (**J**) of blood vessels were increased in K14-Ang1 mice. After UVB irradiation, the change of blood vessel size was smaller in K14-Ang1 mice than in WT mice. The density was comparable in skins exposed and not exposed to UVB ($N = 5$ for each group). $^{*}P < 0.05$, $^{**}P < 0.01$, and $^{***}P < 0.001$. Scale bars = 100 μm.

tin (BD Bioscience) for 1 hour. LECs (100 μL; 1 $\times$ 10^6 cells/mL) in serum-free EBM were seeded into the upper chambers and incubated for 4 hours at 37°C in the presence of Ang1 (5 to 500 μg/mL). The fluorescence intensity (proportional to the number of viable cells) was measured using a Fluoroskan Ascent (Thermo Fisher Scientific, Waltham, MA). Cord-formation assays were performed as described.[19] LECs after transfection of either Tie1, Tie2, or control siRNA were grown on fibronectin-coated 24-well plates until confluence. Then, 0.5 mL of a neutralized isotonic bovine dermal collagen type I solution (Vitrogen, Palo Alto, CA) with or without Ang1 (500 ng/mL) was added to the cells. After incubation at 37°C for 6 hours, cells were fixed with 4% paraformaldehyde for 30 minutes at 4°C. Representative images were captured and the total length of tube-like structures per area was measured using the IP-LAB software, as described.[19] A permeability assay also was performed. Briefly, LECs were grown to confluence on the fibronectin-coated surface of 0.4-μm pore size tissue culture inserts (Corning, Lowell, MA), followed by culture in serum-free EBM for 24 hours. Then, the upper and lower chambers were cultured in the presence or absence of angiopoetin-1 (50 to 500 ng/mL) together with S-nitroso-N-acetylpenicillamine[20](Sigma) for 6 hours. fluorescein isothiocyanate–dextran was added to the upper chambers, and after incubation for 15 minutes the concentration of fluorescein isothiocyanate–dextran in the lower chambers was determined at 492 nm using a Fluoroskan Ascent spectrophotometer (Thermo Fisher Scientific).

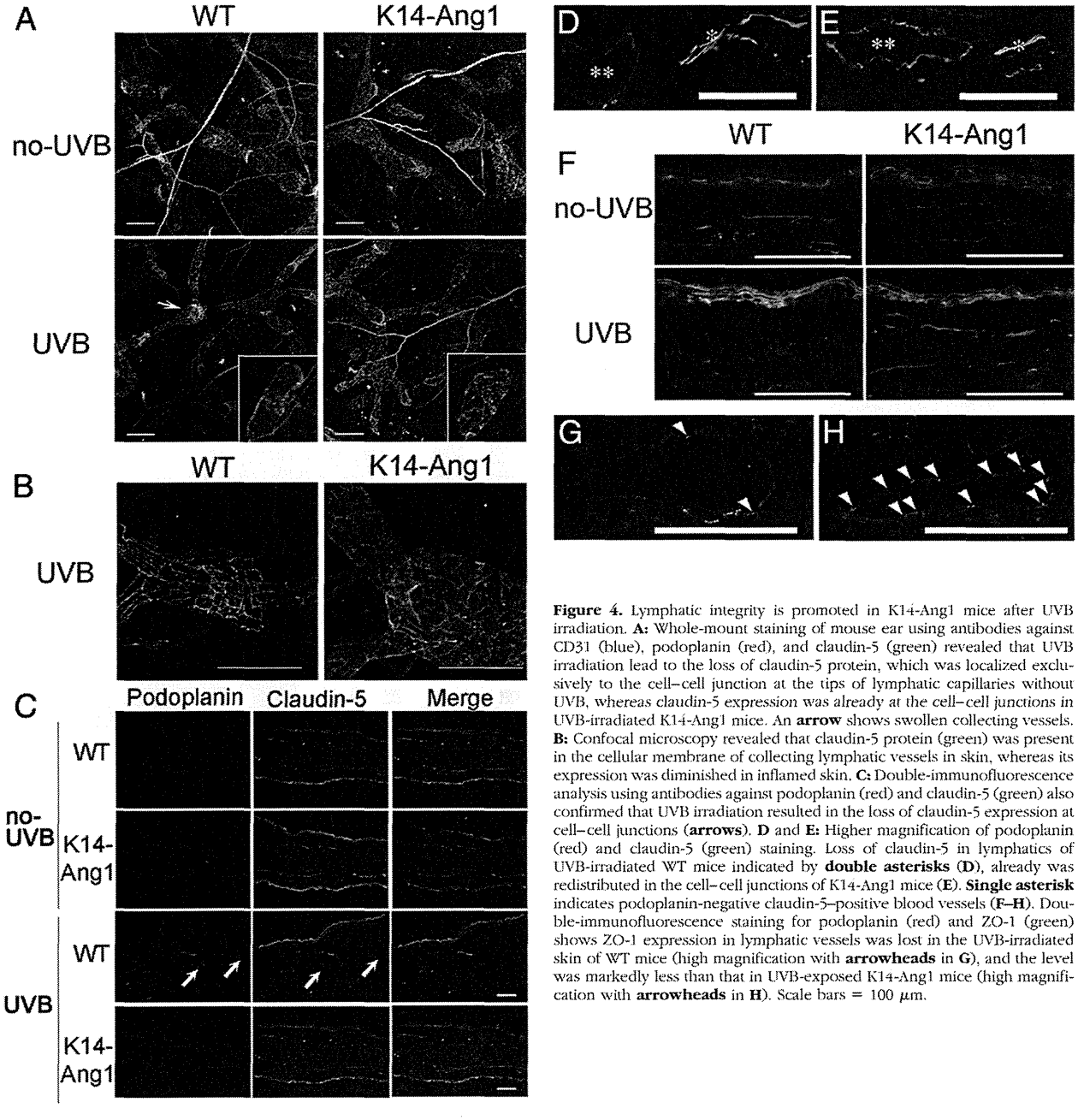

Figure 4. Lymphatic integrity is promoted in K14-Ang1 mice after UVB irradiation. **A:** Whole-mount staining of mouse ear using antibodies against CD31 (blue), podoplanin (red), and claudin-5 (green) revealed that UVB irradiation lead to the loss of claudin-5 protein, which was localized exclusively to the cell–cell junction at the tips of lymphatic capillaries without UVB, whereas claudin-5 expression was already at the cell–cell junctions in UVB-irradiated K14-Ang1 mice. An **arrow** shows swollen collecting vessels. **B:** Confocal microscopy revealed that claudin-5 protein (green) was present in the cellular membrane of collecting lymphatic vessels in skin, whereas its expression was diminished in inflamed skin. **C:** Double-immunofluorescence analysis using antibodies against podoplanin (red) and claudin-5 (green) also confirmed that UVB irradiation resulted in the loss of claudin-5 expression at cell–cell junctions (**arrows**). **D** and **E:** Higher magnification of podoplanin (red) and claudin-5 (green) staining. Loss of claudin-5 in lymphatics of UVB-irradiated WT mice indicated by **double asterisks (D)**, already was redistributed in the cell–cell junctions of K14-Ang1 mice (**E**). **Single asterisk** indicates podoplanin-negative claudin-5–positive blood vessels (**F–H**). Double-immunofluorescence staining for podoplanin (red) and ZO-1 (green) shows ZO-1 expression in lymphatic vessels was lost in the UVB-irradiated skin of WT mice (high magnification with **arrowheads** in **G**), and the level was markedly less than that in UVB-exposed K14-Ang1 mice (high magnification with **arrowheads** in **H**). Scale bars = 100 μm.

Claudin-5–siRNA transfected or control-siRNA transfected LECs also were cultured on the fibronectin-coated surface of 0.4-μm pore size tissue culture inserts for 2 days, followed by incubation in serum-free EBM for 24 hours. Then, fluorescein isothiocyanate was added to the upper chambers and the concentration of fluorescein isothiocyanate in the lower chambers was measured. All studies were performed in triplicate. Statistical analyses were performed using the unpaired Student's *t*-test.

Results

Edema Formation and Inflammation Induced by Acute UVB Irradiation Are Attenuated in K14-Ang1 Mice

To determine the role of Ang1 in cutaneous inflammation, K14-Ang1 mice and WT mice were exposed to 200 mJ/cm^2 of UVB irradiation. Pronounced ear swelling was observed in WT mice, starting at day 2 after UVB irradiation; however, the ear swelling was attenuated significantly in K14-Ang1 mice (Figure 1A). Histologic analysis revealed no major physiological difference between WT mice and K14-Ang1 mice in the absence of UVB exposure (Figure 1, B and C). The ears of UVB-irradiated WT mice showed the characteristics of inflammation, such as epidermal hyperplasia and dermal edema, whereas these changes were ameliorated in K14-Ang1 mice (Figure 1, D and E). Immunohistochemical analysis of a monocyte-macrophage marker, CD11b, indicated marked macrophage infiltration in UVB-exposed WT mouse ear, whereas the number of infiltrated macrophages was decreased in K14-Ang1 mice (Figure 1, H and I). Few or no CD11b-positive macrophages were found in WT or K14-Ang1 mice not exposed to UVB (Figure 1, F and G).

Promotion of Lymphatic and Blood Vascular Function of K14-Ang1 Mice during Inflammation

First, a Miles assay was performed to determine the effects of Ang1 on blood vessels. UVB exposure induced marked leakage of Evans blue dye in WT mice, whereas K14-Ang1 mice showed decreased leakiness, as compared with WT mice (Figure 2A). Quantitative analysis showed that UVB irradiation strongly enhanced dye leakage in WT mouse ear, whereas the increase of dye leakage was inhibited markedly in UVB-irradiated K14-Ang1 mice, although there was still a significant difference between nonirradiated and UVB-irradiated K14-Ang1 mice

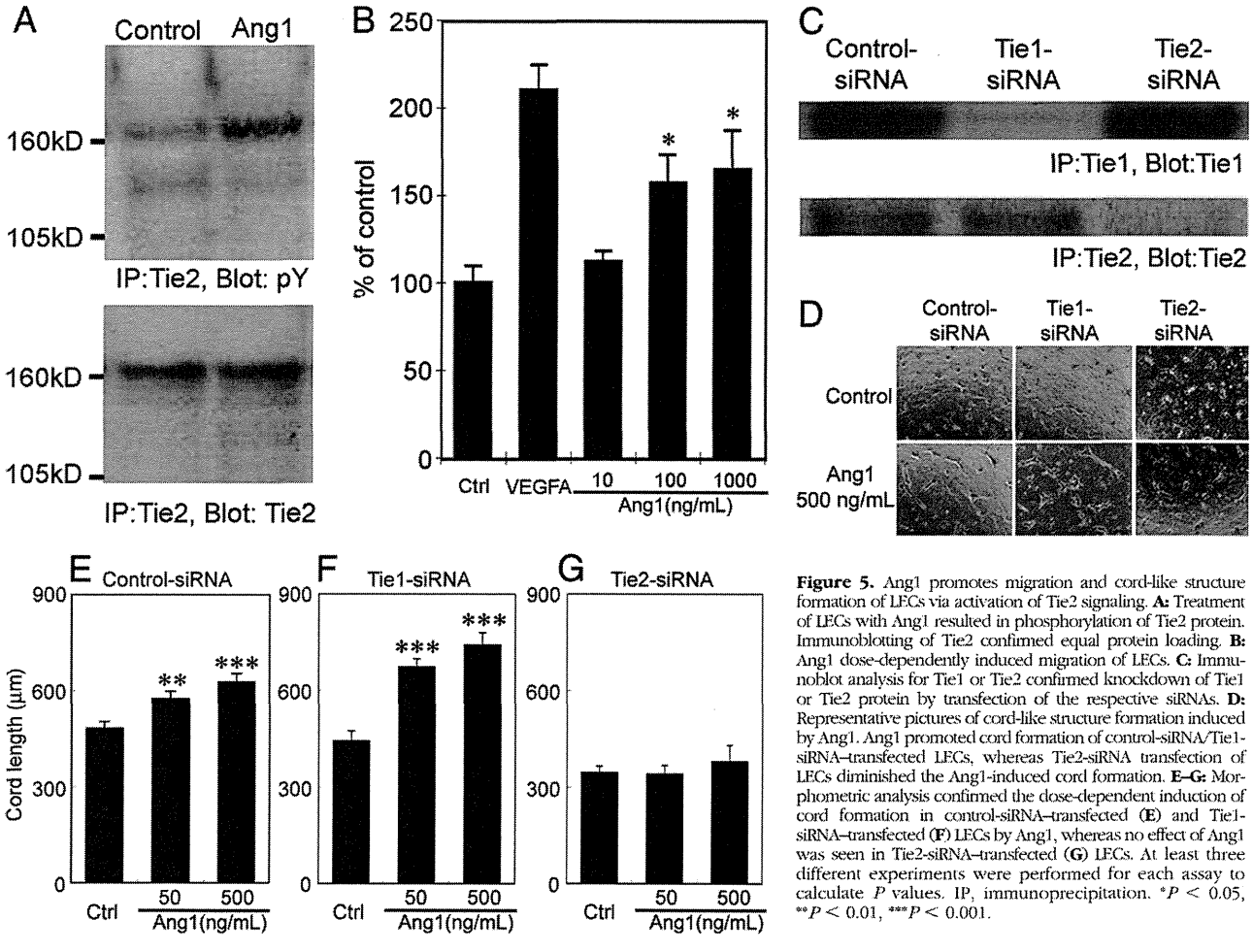

Figure 5. Ang1 promotes migration and cord-like structure formation of LECs via activation of Tie2 signaling. **A:** Treatment of LECs with Ang1 resulted in phosphorylation of Tie2 protein. Immunoblotting of Tie2 confirmed equal protein loading. **B:** Ang1 dose-dependently induced migration of LECs. **C:** Immunoblot analysis for Tie1 or Tie2 confirmed knockdown of Tie1 or Tie2 protein by transfection of the respective siRNAs. **D:** Representative pictures of cord-like structure formation induced by Ang1. Ang1 promoted cord formation of control-siRNA/Tie1-siRNA–transfected LECs, whereas Tie2-siRNA transfection of LECs diminished the Ang1-induced cord formation. **E–G:** Morphometric analysis confirmed the dose-dependent induction of cord formation in control-siRNA–transfected (**E**) and Tie1-siRNA–transfected (**F**) LECs by Ang1, whereas no effect of Ang1 was seen in Tie2-siRNA–transfected (**G**) LECs. At least three different experiments were performed for each assay to calculate *P* values. IP, immunoprecipitation. $^{*}P < 0.05$, $^{**}P < 0.01$, $^{***}P < 0.001$.